

- <sup>4</sup>S. N. Jasperson and S. E. Schnatterly, *Bull. Am. Phys. Soc.* **12**, 399 (1967); J. L. Stanford, H. E. Bennett, J. M. Bennett, E. J. Ashley, and E. T. Arakawa, *ibid.* **13**, 989 (1968).
- <sup>5</sup>B. P. Feuerbacher and W. Steinman, *Opt. Commun.* **1**, 81 (1969).
- <sup>6</sup>J. Endriz and W. E. Spicer, *Phys. Rev. Letters* **24**, 64 (1970).
- <sup>7</sup>J. Endriz and W. E. Spicer, following paper, *Phys. Rev.* **4**, xxxx (1971).
- <sup>8</sup>O. Hunderi and D. Beaglehole, University of Maryland, Department of Physics, Technical Reports Nos. 70-032 and 70-033, 1969 (unpublished).
- <sup>9</sup>D. W. Berreman, *Phys. Rev.* **163**, 855 (1967).
- <sup>10</sup>J. M. Elson and R. H. Ritchie, this issue, *Phys. Rev. B* **4**, xxxx (1971).
- <sup>11</sup>G. Hass, W. R. Hunter, and R. Tousey, *J. Opt. Soc. Am.* **46**, 1009 (1956).
- <sup>12</sup>H. E. Bennett, M. Silver, and E. J. Ashley, *J. Opt. Soc. Am.* **53**, 1089 (1963).
- <sup>13</sup>R. P. Madden, L. R. Canfield, and G. Hass, *J. Opt. Soc. Am.* **53**, 620 (1963).
- <sup>14</sup>R. C. Vehse, E. T. Arakawa, and J. L. Stanford, *J. Opt. Soc. Am.* **57**, 551 (1967).
- <sup>15</sup>O. Hunderi and D. Beaglehole, *Physics Letters* **29A**, 335 (1969).
- <sup>16</sup>U. Fano, *J. Opt. Soc. Am.* **31**, 213 (1941).
- <sup>17</sup>E. A. Stern and R. A. Ferrell, *Phys. Rev.* **111**, 1214 (1958).
- <sup>18</sup>E. A. Stern and R. A. Ferrell, *Phys. Rev.* **120**, 130 (1960).
- <sup>19</sup>V. Twersky, *Trans. IEEE Antennas Propagation AP5*, 81 (1957).
- <sup>20</sup>H. E. Bennett and J. O. Porteus, *J. Opt. Soc. Am.* **51**, 123 (1961).
- <sup>21</sup>H. Davies, *Proc. Inst. Elec. Engrs. (London)* **101**, 209 (1954).
- <sup>22</sup>J. O. Porteus, *J. Opt. Soc. Am.* **53**, 1394 (1963).
- <sup>23</sup>H. E. Bennett (private communication).
- <sup>24</sup>D. Beaglehole (private communication).
- <sup>25</sup>B. Feuerbacher, M. Skibowski, and W. Steinman, *J. Opt. Soc. Am.* **58**, 137 (1968).
- <sup>26</sup>J. Endriz, Ph.D. dissertation (Stanford University, 1970) (unpublished).
- <sup>27</sup>Built by T. DiStefano of this laboratory.
- <sup>28</sup>H. E. Bennett, J. M. Bennett, E. J. Ashley, and R. J. Motyka, *Phys. Rev.* **165**, 755 (1968).
- <sup>29</sup>R. G. Johnston, L. R. Canfield, and R. P. Madden, *Appl. Opt.* **6**, 719 (1967).
- <sup>30</sup>Modified form of the results in Ref. 4 and obtained from J. L. Stanford (private communication).

## Study of Aluminum Films. II. Photoemission Studies of Surface-Plasmon Oscillations on Controlled-Roughness Films\*

J. G. Endriz and W. E. Spicer

*Stanford University, Stanford, California* 94305

(Received 28 April 1971)

Photoemission studies have been conducted on Al films of varied surface roughness. Photoyield measurements indicate very strong peaks at energies approaching the Al surface-plasma frequency, and these peak magnitudes are strongly correlated with surface roughness. This photoyield effect has been interpreted in terms of a two-step process. In the first step, surface roughness allows optical excitation of surface plasmons in accordance with recent surface-plasmon excitation theories. In the second step, the excited plasmons decay into one-electron excitations that can be observed in photoemission. Two mechanisms directly analogous to the volume- and surface-photoeffect theories have been proposed for this plasmon-decay process. The anomalously large values of photoyield per decaying plasmon strongly indicate that the historically significant surface photoeffect is the dominant process giving rise to the observed photoyield effects. An experimental estimate was obtained for the characteristic strength of this surface photoeffect. This estimate was confirmed at a single energy (7.8 eV) in an independent measurement of smooth surface Al photoyield vs angle of incidence for *p*-polarized light. This derived value for the surface-effect strength is believed to provide the first experimental comparisons of the strengths of both surface and volume photoeffects. The high sensitivity of the plasmon-decay process allowed observation of changes in Al photoyield vs time, which were apparently related to changes in film roughness associated with room-temperature annealing. The photoyield effect was highly sensitive to roughness in very smooth films, and a photoyield/(decaying plasmon) approaching 0.3 electrons was observed near the high-*k* plasma frequency in our smoothest Al films. A mathematical surface-roughness model, based on the discrete stepping of the metallic surface in increments of a lattice constant, was proposed to explain this sensitivity.

### I. INTRODUCTION

Although there has been considerable recent in-

terest in both roughness-induced photoyield and roughness-induced optical effects, the main thrust of the studies described in this paper is toward a

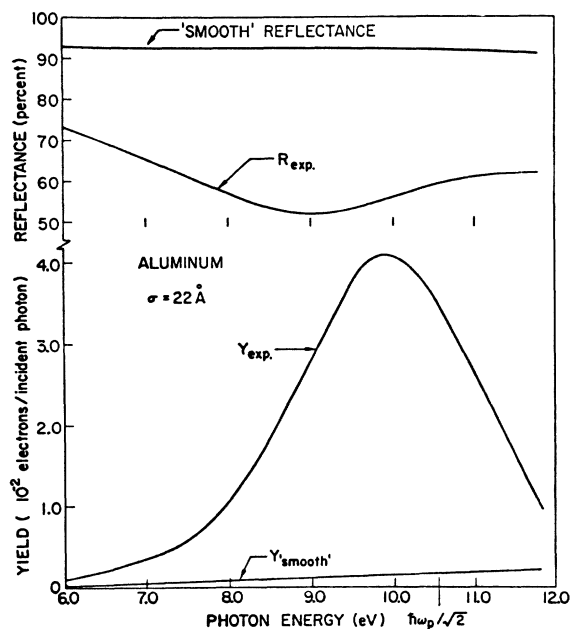


FIG. 1. Reflectance ( $R_{exp}$ ) and photoyield ( $Y_{exp}$ ) from a rough surface Al film. The film roughness was measured and found to have an rms height variation of  $\sigma = 22 \text{ \AA}$ . The smooth surface Al reflectance was determined experimentally, and smooth surface photoyield was estimated from the experimental results described in this paper.

better understanding of roughness-induced photoemission-yield effects. The interpretation of the optical effects described in Paper I<sup>1</sup> serves as a basis.

The most striking aspects of these yield effects are presented in Fig. 1 so that the reader can obtain an immediate appreciation of the nature and magnitude of the phenomenon. The figure compares the photoyield and reflectance measured from the same  $\sigma = 22 \text{ \AA}$  rough aluminum (Al) film to the photoyield and reflectance of smooth Al films. The first effect to be noted is the extraordinary magnitude of the photoyield, which is far greater than the associated reflectance change on the same film. The second effect is the striking correlation of the photoyield increase with the surface-plasma frequency. The plasmon-induced reflectance drops discussed in Paper I were strongly obscured by scattered-light effects and the possibility of roughness-induced anomalous absorption; the photoyield effects discussed in this paper, however, are reasonably well correlated with the surface-plasma frequency, with no clear evidence that the photoyield increase above this frequency is caused by anything other than lifetime broadening of the surface-plasma oscillations. It will be assumed, therefore, that the observed increases in these roughened surfaces are entirely the result of roughness-induced surface-plasmon excitation.

Our principal concern is the determination of the exact process by which roughness-aided surface-plasmon excitation results in an enormous increase in photoyield. The effect was originally observed by Endriz and Spicer<sup>2</sup> and interpreted as a volume photoemission effect associated with the decay of surface plasmons. More extensive experimental photoyield studies and the better understanding of plasmon-induced optical effects reported in Paper I<sup>1</sup> have since indicated that a simple volume-photoemission theory may be insufficient to explain the magnitude of the yield increase.

We will reexamine the theory of the photoyield contribution in the volume-photoemission effect associated with the decay of surface plasmons, and this theory will be modified to include photoyield increases resulting from the decay of plasmons in the historically significant surface photoemission effect.<sup>3,4</sup> These theories will be compared to our optical and photoemission measurements on controlled-roughness Al films. The inability of the volume-photoemission-effect theory to explain our experimental results is stressed, clearly implying that the inclusion of the surface photoemission effect is necessary if these experimental results are to be understood. This observation is believed to be among the strongest pieces of evidence available for the existence of the so-called surface photoemission effect.

Of lesser physical importance but of great practical significance is the extreme sensitivity to surface roughness associated with this plasmon-decay mechanism. We have seen in Fig. 1 that the photoyield effect is far more sensitive to roughness than the reflectance measurements, and this sensitivity is most apparent in the ability to use photoyield measurements to monitor annealing effects in roughened films. This sensitivity is also apparent in residual roughness effects—the inability to eliminate completely the plasmon effect in the photoyield near the surface-plasma frequency of vacuum-evaporated Al films. Practical aspects of both the annealing and “residual-roughness” effects will be discussed in detail.

## II. THEORY OF SURFACE-PLASMON-INDUCED PHOTOYIELD INCREASES

The process of roughness-aided optical excitation of surface plasmons was discussed in Paper I.<sup>1</sup> Here, we are concerned with the exact nature of the subsequent decay of those plasmons. Physically, the lifetime broadening of surface plasmons included in the Elson-Ritchie<sup>5</sup> theory is associated directly with the penetration of the surface-plasmon fields into the volume of a metal (e.g., Al) having finite  $\epsilon_2$  and thus finite loss. The exact nature of the associated plasmon fields is best derived from the theory of surface-plasma oscillations described

by Crowell and Ritchie.<sup>6</sup> In that development, plasma oscillations were described in a free-electron-like metal in which so-called hydrodynamic dispersion effects were included.<sup>1</sup> Within these approximations, the plasmon fields inside the metal ( $z > 0$ ) can be shown to equal

$$\begin{aligned} \vec{E}(\vec{\rho}, z) = & E_0 \frac{\Gamma}{k} \frac{\nu^+}{\nu^+ + \nu^-} \frac{k^2 + \nu^- \Gamma}{\Gamma^2 - k^2} \\ & \times e^{i\vec{k} \cdot \vec{\rho}} e^{-\nu^+ z} \left[ \frac{\vec{k}}{|\vec{k}|} + i \left( \frac{k}{\nu^+} \right) \vec{i}_z \right] \\ & - E_0 \frac{\Gamma}{\Gamma^2 - k^2} e^{i\vec{k} \cdot \vec{\rho}} e^{-\Gamma z} (\vec{k} + i\Gamma \vec{i}_z), \quad (1a) \end{aligned}$$

and outside the metal ( $z < 0$ ) they can be shown to equal

$$\begin{aligned} \vec{E}(\vec{\rho}, z) = & E_0 \frac{\Gamma}{k} \frac{\nu^-}{\nu^+ + \nu^-} \frac{\nu^+ \Gamma - k^2}{\Gamma^2 - k^2} \\ & \times e^{i\vec{k} \cdot \vec{\rho}} e^{\nu^- z} \left[ \frac{\vec{k}}{|\vec{k}|} - i \left( \frac{k}{\nu^-} \right) \vec{i}_z \right], \quad (1b) \end{aligned}$$

where  $\vec{k}$  is the wave vector of the plasmon whose fields are being described,  $\vec{\rho}$  is the position vector directed parallel to the metallic surface,  $z$  is perpendicular to the metallic surface,  $\vec{i}_z$  is the unit vector normal to the surface,  $\nu^+$  is the coefficient for the decay of the plasmon field into the metal where  $(\nu^+)^2 \equiv k^2 + (\omega_p^2 - \omega^2)/c^2$ ,  $\nu^-$  is the coefficient for the decay of the plasmon field into the vacuum where  $(\nu^-)^2 \equiv k^2 - \omega^2/c^2$ , and  $\Gamma$  is the coefficient for plasmon surface-polarization charge decay where  $\Gamma^2 \equiv (\omega_p^2 - \omega^2 + \beta^2 k^2)/\beta^2$ . The quantity  $\omega_p$  is the free-electron plasma frequency, and  $\beta$  is the hydrodynamic velocity of propagation for the electron gas (on the order of the Fermi velocity). For a high- $k$  plasmon ( $k > \omega_p/c$ ), the configuration of these fields is shown in Fig. 2.

It can be seen from Eqs. (1) and Fig. 2 that the plasmon-field penetration depth into the metal  $(\nu^+)^{-1}$  is comparable to the optical penetration depth  $2\alpha^{-1}$  for most plasma wave vectors commonly excited on real surfaces. A photoemission process similar to the normal optical photoemission process, therefore, should be observable as the surface plasmons

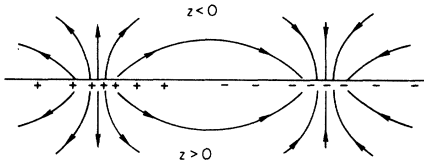


FIG. 2. Surface-plasmon field configurations. The example is a high- $k$  plasmon for which the fields are symmetric about the surface outside ( $z < 0$ ) and inside ( $z > 0$ ) the metal.

decay. An understanding of this plasmon-decay photoemission process depends on a complete understanding of the photoemission process itself; in particular, the peculiar nature of the surface-plasmon fields (their complicated polarization and concentration near the surface for high- $k$  plasmons) motivated our reexamination of the theory of photoemission for the commonly accepted volume mode of photoemission and for the less commonly identified but historically significant surface effect.

Early theories of photoemission in metals<sup>3,4,7</sup> assumed that real metals were well described by the Sommerfeld model and that momentum conservation in an optical excitation could occur only at the surface of the metal. Fan<sup>8</sup> later observed that momentum-conserving electronic interactions with the metallic lattice could be quite strong in real metals. It was believed that so-called direct-transition photoexcitation within the volume of a metal could result in photoemission comparable to the surface-effect photoemission. In recent years, Spicer<sup>9</sup> and others have argued that volume-effect photoemission dominates in virtually all photoemission studies in which, as is usually the case, near-normal-incidence light is used to excite the medium. In the following discussion, we review the theories of volume- and surface-effect photoemission and derive theoretical expressions for the photoyield enhancement to be expected from the surface-plasmon decay.

#### A. Surface-Plasmon-Decay Volume Photoemission Effect

The derivation of the volume photoemission effect follows the work of Spicer.<sup>9</sup> It is assumed that the fraction of photons absorbed per normally incident photon is given by  $1 - R(\hbar\omega)$ , where  $R(\hbar\omega)$  is the normal-incidence reflectance. If the medium is characterized by an optical absorption coefficient  $\alpha(\hbar\omega)$ , one can assume that the field-energy distribution of these absorbed photons is given by  $e^{-\alpha z}$ , with  $z$  normal to the surface. If it is further assumed that photoexcitation is the dominant photon-absorption process and that this process is proportional to the energy density of the exciting optical fields, one can conclude that the distribution of photoexcited electrons per absorbed photon is given by  $D(z) = \alpha e^{-\alpha z}$ . If the probability that an electron excited at point  $z$  will reach the surface is  $\frac{1}{2}e^{-z/l}$ , with  $l$  the electron escape depth (sometimes equal to the electron inelastic scattering length), then the total number of electrons per absorbed photon reaching the surface is equal to  $\frac{1}{2} \times [\alpha l / (1 + \alpha l)]$ .<sup>10</sup> The number of photoemitted electrons, therefore, is related to the escape probability  $P_{es}(E)$  for an electron excited to a final energy  $E$ . An expression for the yield per incident photon then is obtained by integrating over all final

electron energies:

$$Y_{\text{vol}}(\hbar\omega) = [1 - R(\hbar\omega)] \frac{\alpha l}{1 + \alpha l} \int \frac{1}{2} n_{\hbar\omega}(E) P_{\text{es}}(E) dE, \quad (2)$$

where  $l$ , which varies with  $E$ , is assumed to be assigned a mean value over this range of variations, thus allowing its removal from the integral over  $E$ . This simplification is not crucial to our analysis.

In the above integral,  $n_{\hbar\omega}(E)$  is the normalized internal energy distribution of photoexcited electrons for excitation energy  $\hbar\omega$ . This is one form of the so-called volume theory of photoemission.

In addition to the above explicit assumptions, the implicit assumption has been made that an electron excitation at point  $z$  is related to the energy density only at point  $z$ . This assumption is valid only if  $\alpha l_p \ll 1$ , where  $l_p$  is the excitation dephasing distance, and its breakdown is similar to the anomalous skin effect. The above derivation in terms of arbitrary  $\alpha l$  (possibly  $> 1$ ) thus implies  $l_p \ll l$  or a dephasing length  $l_p$  which can be much less than the electron escape depth.

This theory of volume-effect photoemission can be extended to the interpretation of observed surface-plasmon-induced photoyield increases. For surface oscillations having wave vectors in or near the retardation region (Fig. 1, Paper I),  $\beta$  can be assumed very small in the field expressions of Eq. (1). In this limit, the fields within the metal reduce to a simple expression whose field magnitude is proportional to  $e^{-\nu^* z}$  [see also Eq. (10)].

In polycrystalline materials or materials having a cubic crystal structure, the difference in the polarization of the exciting optical or plasmon fields may be assumed small in the volume theory. The excitation of the medium associated with the plasmon fields thus is analogous to the excitation of the metal by optical fields, with the optical absorption coefficient  $\alpha$  replaced by the plasmon-field decay coefficient  $2\nu^*$ . If the fraction of incoming photons absorbed by plasmons of wave vector  $k$  is denoted by  $\Delta R_k(\hbar\omega)$ , the increase in photoyield associated with the decay of these particular plasmons is

$$\Delta Y_k(\hbar\omega) = \Delta R_k(\hbar\omega) \frac{2\nu^* l}{1 + 2\nu^* l} \int \frac{1}{2} n_{\hbar\omega}(E) P_{\text{es}}(E) dE. \quad (3)$$

The fractional increase in photoyield  $\Delta Y_k(h\nu)$  can be expressed in the simple form of

$$\frac{\Delta Y_k(\hbar\omega)}{Y_{\text{vol}}(\hbar\omega)} = \frac{\Delta R_k(\hbar\omega)}{1 - R(\hbar\omega)} \frac{2\nu^*}{\alpha} \frac{1 + \alpha l}{1 + 2\nu^* l}, \quad (4)$$

which can be interpreted as the fractional increase in photons absorbed by the metal and modified by the effects of the ratio of optical-to-surface-plas-

mon field penetration depths. The total increase in photoyield at incoming photon excitation energy  $\hbar\omega$ , therefore, can then be expressed as an integral over the relative yield increases stemming from the excitation of each of the various plasmons in the plasmon spectrum. The excitation probabilities of various plasmons follows from the Elson-Ritchie<sup>5</sup> expression of Eq. (3) in Paper I. For the total increase in photoyield, this expression can be combined with Eq. (4) and integrated to yield

$$\frac{\Delta Y(\hbar\omega)}{Y_{\text{vol}}(\hbar\omega)} = \frac{1}{\Delta R(\hbar\omega)} \frac{\sigma^2 \omega^3}{2\pi c^2} \int_0^\infty F(\epsilon_1, \omega_k) \frac{2\nu^*}{\alpha} \frac{1 + \alpha l}{1 + 2\nu^* l} \times \frac{k}{P_k} \frac{\gamma_k}{(\omega - \omega_k)^2 + (\frac{1}{2} \gamma_k)^2} g(k) dk, \quad (5)$$

where

$$F(\epsilon_1, \omega_k) = \frac{1}{1 - \epsilon_1} \left\{ 3(\epsilon_1 - 1) + \omega_k \frac{d\epsilon_1}{d\omega} \left[ 1 - \left( \frac{\epsilon_1 + 1}{\epsilon_1} \right)^{1/2} \right] \right\}^2.$$

In Paper I,  $P_k$ ,  $\omega_k$ ,  $\gamma_k$ ,  $\sigma$ , and  $g(k)$  are defined precisely, and  $\Delta R(\hbar\omega) = 1 - R(\hbar\omega)$ . The expected reflectance drop associated with a rough Al surface characterized by a Gaussian autocorrelation function with rms height variation  $\sigma = 15 \text{ \AA}$  and autocorrelation length  $\bar{a} = 450 \text{ \AA}$  was plotted in Fig. 2 of Paper I. This same reflectance drop is replotted in Fig. 3 of this paper; also shown are the smooth surface Al photoyield and the increase in photoyield expected from the volume theory of Eq. (5), assuming that the surface-roughness spectrum  $\sigma^2 g(k)$  is well described by this same Gaussian roughness spectrum. This calculation of the surface-plasmon-decay volume photoemission effect assumes that the electron inelastic scattering length  $l$  is  $70 \text{ \AA}$  (see Sec. IV).

The important aspects of this mechanism can be qualitatively appreciated in Fig. 3. Because the relative increase in photoyield is proportional to  $[\Delta R(\hbar\omega)]^{-1}$  ( $\Delta R \equiv 1 - R$ , where  $R$  is the smooth surface reflectance), the photoyield effect can be large in nearly free-electron highly reflecting metals such as Al. The slight enhancement in the photoyield per absorbed photon also is noted in this volume-effect theory as one approaches the high- $k$  plasmon frequency where the field penetration-depth ratio  $(2\nu^*/\alpha) [(1 + \alpha l)/(1 + 2\nu^* l)]$  begins to affect the yield.

#### B. Surface-Plasmon-Decay Surface-Effect Photoemission

Surface-effect photoemission was first proposed by Tamm and Schubin,<sup>3</sup> Fröhlich,<sup>7</sup> Mitchell,<sup>4,11</sup>

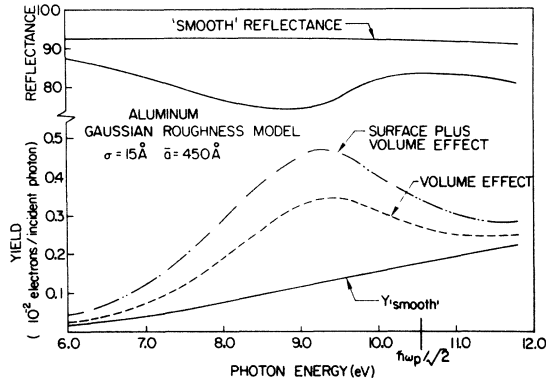


FIG. 3. Theoretical plasmon-induced photoyield increases for Al. The increases are calculated in the volume-effect photoemission and surface-plus volume-effect photoemission theories, assuming a rough surface having a Gaussian surface-height autocorrelation function characterized by a rms height variation of 15 Å and an autocorrelation length of 450 Å. Also included are plots of the experimentally determined smooth surface Al reflectance and photoyield, as well as the Al reflectance drop calculated for this Gaussian surface in the plasmon-coupling light-scattering theory of Elson and Ritchie.

and others in an attempt to explain the observed photoemission in metals thought to be well described (in the Sommerfeld model) by a free-electron gas in which electronic interaction with the lattice can be ignored. Of necessity momentum conservation in an optical excitation then must occur at the metallic surface. Because the surface-potential discontinuity exists only in the dimension normal to the surface, momentum transfer can exist only normal to the surface and only if the optical excitation has a field component normal to the surface. Clearly, surface-effect photoemission can occur only if the exciting optical field is at non-normal incidence or arises from some mechanism that yields a field component normal to the surface. The region over which the optical coupling can appear is related to the distance over which the electronic wave functions are distorted from their volume values. Although various forms have been assumed for the surface-potential discontinuity, many of them result in a distortion of wave functions that begins within a few angstroms of the surface and extends a few angstroms outside of the metal; unfortunately, these distances are comparable to the distance over which one passes from the incident and reflected light waves to the transmitted light wave,<sup>12</sup> which severely complicates the problem of determining the excitation fields inducing the surface photoeffect.

Mitchell<sup>4,11</sup> has calculated optically induced surface-effect photoemission in two simplifying limits: One of which assumes that the optical-excita-

tion fields change so slowly near  $z=0$  that the excitation fields can be approximated by the incident-plus-reflected optical fields over the entire surface-excitation region; the second of which assumes an instantaneous change from incident and reflected waves to a transmitted wave at  $z=0$ . It is not clear which of these approximate calculations is preferable but, at worst, they both offer solutions that differ, at most, by a factor of 2.

For simplicity, the first model, which assumes that the incident-plus-reflected light waves yield the appropriate surface-photoeffect excitation fields, has been selected. As a result, the normal component of the field, important in the surface-effect photoexcitation process, is approximated by  $\vec{a}_{xi} + \vec{a}_{xr}$  which is the normal component of the incident-plus-reflected field, as calculated classically from the optical constants of the metal. The surface-effect photoemission, therefore, is proportional to the square of this normal component of the excitation field times a characteristic surface-effect strength that depends on the details of the surface-potential discontinuity. The surface effect can be expressed as the photoyield/incident photon by normalizing the photoemission current to the incident photon flux  $(\omega/hc)|\vec{a}_i|^2$ , where  $\vec{a}_i$  is the incident vector-potential-field strength. Expressed in this form, the surface photoemission strength is

$$Y_{\text{surface}}(\hbar\omega) = \left( \frac{|\vec{a}_{xi} + \vec{a}_{xr}|^2}{|\vec{a}_i|^2} \right) Y_c(\hbar\omega), \quad (6)$$

where  $Y_c(\hbar\omega)$  represents the characteristic surface-effect photoemission per incident photon that would occur if the incident field strength is directed

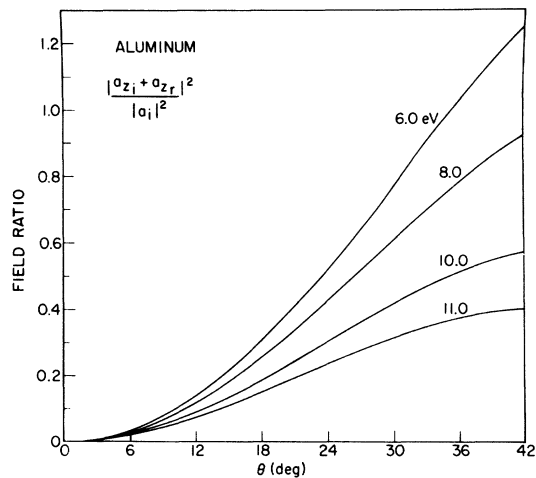


FIG. 4. Field ratios for  $p$ -polarized light. Shown is the ratio of field component normal to the surface squared to incident field strength squared for a  $p$ -polarized light beam incident on a smooth Al surface at various angles and for various light-beam energies.

perpendicular to the surface. Figure 4 is an example of the strong quadratic dependence of surface-effect photoemission on angle-of-light incidence in plots of  $|\vec{a}_{st} + \vec{a}_{sr}|^2 / |\vec{a}_t|^2$  vs angle-of- $p$ -polarized-light incidence for Al.

As defined in Eq. (6),  $Y_c(\hbar\omega)$  is independent of the angle of incidence of light or the reflection and refraction of light at the surface, and it is characteristic only of the surface potential discontinuity. For example, Mitchell's earliest calculation of surface-effect photoemission strength<sup>4</sup> assumes a step function potential discontinuity and a free-electron model which, for  $Y_c(\hbar\omega)$ , yields

$$Y_c(\hbar\omega) = \frac{2\hbar\omega_0 e^3}{\pi cm^2 \omega^3} \int_0^{k_F} dk_x \times \frac{k_x^2 (k_F^2 - k_x^2) [k_x^2 + (k_x^2 - k_a^2)]^2}{\{[k_x^2 + k_\omega^2]^{1/2} + [k_x^2 + (k_x^2 - k_a^2)]^{1/2}\}^2}, \quad (7)$$

where  $\hbar\omega_0$  is the vacuum level as measured from the bottom of the conduction band,  $k_a^2$  is defined as  $4\pi m\omega_0/h$ ,  $k_F$  is the Fermi wave number, and  $k_\omega^2$  is defined as  $4\pi m\omega/h$ . This expression is a function

$$\frac{Y_s(\theta, \hbar\omega)}{Y_{\text{vol}}(\theta, \hbar\omega)} = \left( \frac{|\vec{a}_{st} + \vec{a}_{sr}|^2}{|\vec{a}_t|^2} \right)^2 Y_c(\hbar\omega) / \left\{ \frac{\alpha(\theta) \Delta R(\theta, \hbar\omega)}{\alpha(0) \Delta R(0, \hbar\omega)} \frac{1 + \alpha(0)l}{1 + \alpha(\theta)l} \right\} Y_{\text{vol}}(0, \hbar\omega) \Bigg\} \\ \equiv \left( \frac{|\vec{a}_{st} + \vec{a}_{sr}|^2}{|\vec{a}_t|^2} \right)^2 \left[ \frac{\alpha(0) \Delta R(0, \hbar\omega) [1 + \alpha(\theta)l]}{\alpha(\theta) \Delta R(\theta, \hbar\omega) [1 + \alpha(0)l]} \right] R_c(\hbar\omega), \quad (8)$$

where  $R_c(\hbar\omega) \equiv Y_c(\hbar\omega)/Y_{\text{vol}}(0, \hbar\omega)$ , and the dependence of the volume photoeffect on angle-of-light incidence has been included by expressing the parameters  $\Delta R \equiv 1 - R$  and  $\alpha$  [from Eq. (2)], as functions of angle. Substituting Eq. (2) into (8), we obtain

$$\frac{Y_s(\theta, \hbar\omega)}{Y_{\text{vol}}(\theta, \hbar\omega)} = \left[ \frac{|\vec{a}_{st} + \vec{a}_{sr}|^2}{|\vec{a}_t|^2} \frac{1 + \alpha(\theta)l}{\alpha(\theta)l \Delta R(\theta, \hbar\omega)} \right] \times \left[ \frac{Y_c(\hbar\omega)}{\int \frac{1}{2} n_{\hbar\omega}(E) P_{\text{es}}(E) dE} \right]. \quad (9)$$

This equation is divided conveniently into a factor  $Y_c / \int \frac{1}{2} n_{\hbar\omega}(E) P_{\text{es}}(E) dE$  relating to the work function, escape function, and the details of the surface-photoemission-effect strength, and a factor

$$\left[ \frac{|\vec{a}_{st} + \vec{a}_{sr}|^2}{|\vec{a}_t|^2} \frac{1 + \alpha(\theta)l}{\alpha(\theta)l \Delta R(\theta, \hbar\omega)} \right]$$

entirely derivable from the optical constants of the material, angle of incidence of light on the surface, light polarization, and electron inelastic scattering length  $l$ . It is interesting to note that

only of the surface-potential model, vacuum-level energy, and metallic Fermi energy. It should be noted that this is a rather primitive surface effect model; because it does not obtain good quantitative agreement with experiment, it should be considered as a theoretical example of the type of processes that gives rise to surface-effect photoemission.

In real metals, photoexcitation can occur via both the volume and surface processes. Schach and Ashcroft<sup>13</sup> pointed out that interference effects occur between these two processes, and they cannot be added simply. However, this fact is ignored in this paper. Interference effects occur for specific final electron energies and/or angles of emission. Ours are photoyield measurements over all emitted-electron angles and energies so that such effects are possibly averaged out. In any case, the results described in this discussion should remain strictly valid in the limit for which either the volume or surface effect dominates the photoemission. Assuming that the surface and volume effects are separable leads to a useful and descriptive expression for the ratio of surface-effect-to-volume-effect photoemission:

the latter allows one to determine a great deal concerning the expected ratio of surface-effect-to-volume-effect photoemission for various metals without any knowledge of the details of the surface potential. For example, both the case of a completely free-electron metal (for which the ratio  $Y_s/Y_{\text{vol}}$  is  $\infty$ ) and the case of normal light incidence (for which the ratio  $Y_s/Y_{\text{vol}}$  is 0) are described only by this factor. Figure 5 is a plot of the characteristic surface-effect strength  $Y_c(\hbar\omega)$ , calculated from Mitchell and used in sample calculations plotted in Figs. 3, 6, 7, and 13; also shown is  $R_c(\hbar\omega)$ , which is the ratio of  $Y_c(\hbar\omega)$  to our experimental estimate of the normal-incidence smooth surface Al photoyield.

An extension of the theory of surface-effect photoemission to the interpretation of plasmon-induced photoyield effects must begin with a discussion of the surface-plasmon fields. As noted in Sec. II A, the plasmon wave vectors commonly excited on real surfaces are such that  $\beta$  is small and  $\Gamma \gg k$ , so that the fields of Eq. (1) can be approximated by

$$\vec{E}(\vec{\rho}, z) = E_0 \frac{\nu^+ \nu^-}{\nu^+ + \nu^-} e^{i\vec{k} \cdot \vec{\rho}} e^{-\nu^+ z}$$

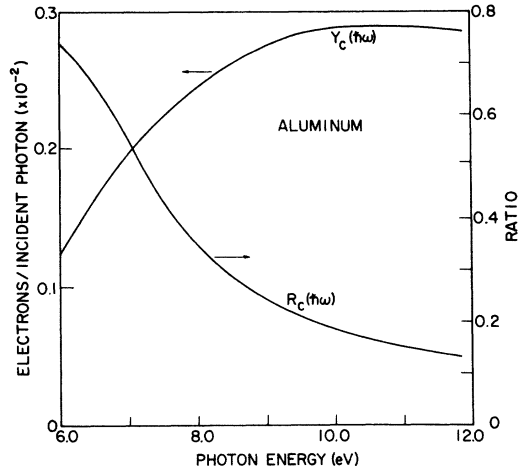


FIG. 5. The characteristic surface-effect strength  $Y_c(\hbar\omega)$  and ratio  $R_c(\hbar\omega)$  calculated as an example of surface-effect photoemission using Mitchell's model and Al parameters. The volume-effect photoemission used in calculating  $R_c(\hbar\omega)$  is the smooth surface Al photoyield estimated from experiment.

$$\times \left[ \frac{1}{k} \frac{\vec{k}}{|\vec{k}|} + i \left( \frac{1}{\nu^+} \right) \vec{i}_s \right] \text{ for } z > 0 \quad (10a)$$

$$= E_0 \left( \frac{\nu^+ \nu^-}{\nu^+ + \nu^-} \right) e^{i\vec{k} \cdot \vec{\rho}} e^{\nu^- z}$$

$$\times \left[ \frac{1}{k} \frac{\vec{k}}{|\vec{k}|} - i \left( \frac{1}{\nu^-} \right) \vec{i}_s \right] \text{ for } z < 0. \quad (10b)$$

The critical aspect of these fields is the strong field component that occurs normal to the surface [Eqs. (1) and (10) and Fig. 2]. *Surface roughness allows a normally incident optical excitation with very weak field components normal to the surface to launch surface waves having strong normal field components.* The precise strength of the surface-effect photoyield in the plasmon-decay process is related directly to the strength of these normal field components near  $z = 0$ . In determining these plasmon fields in the region of the surface, a difficulty arises<sup>14</sup> that is exactly analogous to the difficulty found in optical excitation of the surface photoeffect. Consistent with the assumption in the solution of the optical problem, we have assumed that the appropriate plasmon fields are those fields located only on the vacuum side of the surface ( $z = 0^-$ ).

This field strength of a plasmon having wave vector  $k$  can be determined simply if the plasmon energy loss or decay is assumed still to be primarily caused by electron excitation within the *volume* of the metal. Note that this is distinct from assuming that the volume photoeffect dominates the photoemission. Surface effects can dominate the

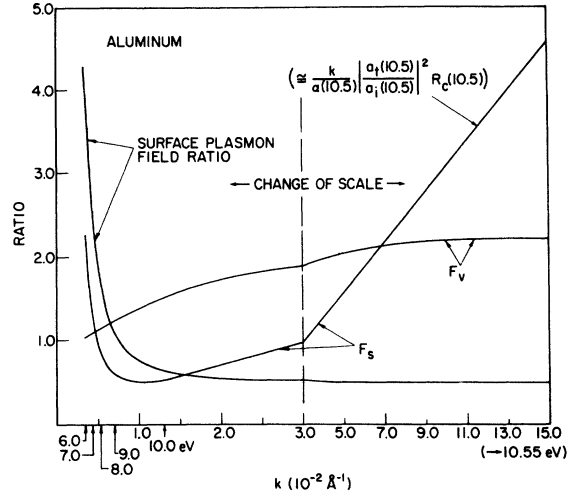


FIG. 6. Surface-effect ( $F_s$ ) and volume-effect ( $F_v$ ) surface-plasmon photoyield enhancement factors. These factors obtain the theoretical enhancement in photoyield per decaying plasmon over the photoyield per absorbed photon for normally incident light on a smooth Al surface. The ratios are plotted vs plasmon wave vector, with corresponding plasmon energies also shown on the wave-vector axis. The Mitchell model was used in calculating  $F_s$ . The surface-plasmon field ratio  $k^2(\nu^+)^2/(\nu^-)^2 \times [(\nu^+)^2 + k^2]$  is crucial in calculating  $F_s$  and is plotted separately.

photoemission even though the plasmon energy loss occurs primarily in the volume of the metal. This assumption probably is valid for all but the highest- $k$  plasmons optically excited on real surfaces. Within this volume energy-loss assumption, the ratio of plasmon-to-optical-excitation field strength squared just inside the metallic surface

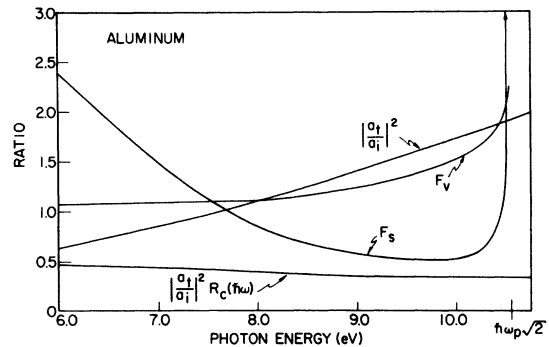


FIG. 7. Surface-effect ( $F_s$ ) and volume-effect ( $F_v$ ) surface-plasmon enhancement factors vs photon (plasmon) energy. Also shown are the optical-transmission factor  $|\vec{a}_t/\vec{a}_i|^2$  and the factor  $(|\vec{a}_t/\vec{a}_i|^2)R_c(\hbar\omega)$ , as calculated using the Mitchell model; both are factors in calculating  $F_s$ . As in Fig. 6, the enhancement factor  $F_v$  saturates at  $< 2.5$ , whereas the  $F_s$  continues to grow for high- $k$  plasmons. The electron escape depth of 70 Å used in calculating  $F_v$  was estimated from experiment.

( $z=0^+$ ) is the ratio of absorbed photons  $\Delta R_k(\hbar\omega)/\Delta R(\hbar\omega)$  times an energy-density-concentration ratio  $2\nu^*/\alpha$ . It can be seen from Eq. (10) that the ratio of plasmon-field strength squared normal to the surface at  $z=0^-$  to plasmon-field strength squared at  $z=0^+$  is  $k^2(\nu^*)^2/(\nu^-)^2[(\nu^*)^2+k^2]$ . The ratio of field strength normal to the surface squared to field strength squared for an optical excitation at  $z=0^+$ , therefore, is

$$\frac{\Delta R_k(\hbar\omega)}{\Delta R(\hbar\omega)} \frac{2\nu^*}{\alpha} \frac{k^2(\nu^*)^2}{(\nu^-)^2[(\nu^*)^2+k^2]}.$$

If  $Y_c(\hbar\omega)$  [Eq. (6)] is defined as the photoyield per incident photon that would occur if the incident field strength is directed normal to the surface, then the plasmon-induced surface photoemission can be expressed in terms of the general surface-effect photoemission strength  $Y_c(\hbar\omega)$  as

$$\Delta Y_k(\hbar\omega) = \frac{\Delta R_k(\hbar\omega)}{\Delta R(\hbar\omega)} \frac{2\nu^*}{\alpha} \frac{k^2(\nu^*)^2}{(\nu^-)^2[(\nu^*)^2+k^2]} \times \frac{|\vec{a}_z(0^+)|^2}{|\vec{a}_z|^2} Y_c(\hbar\omega), \quad (11)$$

where the ratio  $|\vec{a}_z(0^+)|^2/|\vec{a}_z|^2 \equiv |\vec{a}_z|^2/|\vec{a}_z|^2$  is the simple transmission for a normally incident optical excitation and can be calculated from optical constants.

If it is again assumed that the surface- and volume-photoemission effects are separable, then for the total relative photoyield increase associated with both surface- and volume-photoemission effects in the decay of a surface plasmon of wave vector  $k$

$$\frac{\Delta Y_k(\hbar\omega)}{Y_{\text{vol}}(\hbar\omega)} = \frac{\Delta R_k(\hbar\omega)}{\Delta R(\hbar\omega)} \left[ \frac{2\nu^*}{\alpha} \frac{1+\alpha l}{1+2\nu^* l} + \frac{2\nu^*}{\alpha} \frac{k^2(\nu^*)^2}{(\nu^-)^2[(\nu^*)^2+k^2]} \frac{|\vec{a}_z|^2}{|\vec{a}_z|^2} R_c(\hbar\omega) \right]. \quad (12)$$

Before generalizing this expression to include plasmon-lifetime effects and integrated effects over all possible plasmons, the various factors in Eq. (12) should be examined to determine under what circumstances the surface- or volume-photoemission effect dominates. The leading factor is a photon-absorption ratio, modified by what is called the "volume enhancement" factor

$$F_v \equiv \frac{2\nu^*}{\alpha} \frac{1+\alpha l}{1+2\nu^* l}$$

and the "surface enhancement" factor

$$F_s \equiv \frac{2\nu^*}{\alpha} \frac{k^2(\nu^*)^2}{(\nu^-)^2[(\nu^*)^2+k^2]} \frac{|\vec{a}_z|^2}{|\vec{a}_z|^2} R_c(\hbar\omega).$$

These two factors and the plasmon-field ratio factor,  $k^2(\nu^*)^2/(\nu^-)^2[(\nu^*)^2+k^2]$ , are plotted as a function

of plasmon wave vector in Fig. 6. Once again the Mitchell<sup>4</sup> calculation for  $Y_c$  and thus  $R_c$  (for Al parameters) has been chosen as an example for evaluating  $F_s$ . It should be reemphasized that this Mitchell model is of limited accuracy and is used primarily as a vehicle for describing the theory of plasmon decay in the surface-excitation theory. Because of this limited accuracy, the characteristic surface-effect strength derived in this paper was obtained from a direct fit to experiment rather than from calculations in the Mitchell theory. The important aspects of the curves in Fig. 6 are independent of the exact form for  $R_c(\hbar\omega)$ .

The volume enhancement factor  $F_v$  saturates to a relatively small value,  $(\alpha l + 1)/\alpha l$  for large plasmon wave vectors (large  $\nu^*$ ). Physically, the photoyield enhancement associated with the concentration of plasmon-field energy nearer the surface is not significant in the volume-photoeffect theory when the plasmon-field decay length becomes less than the relatively large electron escape depth ( $l \approx 70 \text{ \AA}$ ); when the plasmon-field decay length becomes short enough so that all electrons excited are able to reach the surface, this penetration depth enhancement ceases.

Field-penetration depth enhancement in the surface-photoemission effect is quite different. An effective electron escape depth in the surface theory is on the order of a lattice constant; therefore, the enhancement factor  $F_s$  may continue to grow even for high- $k$  plasmons and saturates at only the highest- $k$  values. The asymptotic behavior of  $F_s$  for high- $k$  plasmons is shown in Fig. 6. The surface-photoemission-effect enhancement factor also shows a distinct enhancement effect for low- $k$  plasmons. For short- $k$  plasmons in the retardation region (the corresponding plasmon energies are marked on the  $k$  axis of Fig. 6), the plasmon fields are gradually excluded from the metal as the plasmon fields become similar to a free electromagnetic wave traveling parallel to but outside of the metallic surface. In this low- $k$  limit, the plasmon-field ratio  $k^2(\nu^*)^2/(\nu^-)^2[(\nu^*)^2+k^2]$  becomes large, causing  $F_s$  to increase.

These same factors ( $F_v$  and  $F_s$ ) are plotted according to plasmon energy in Fig. 7; the Mitchell expression for  $R_c(\hbar\omega)$  is again used as our surface model. These curves show the slight enhancement in  $F_v$ , saturating at  $\approx 2.25$ , as one approaches  $\hbar\omega = \hbar\omega_p/\sqrt{2}$  and the high- $k$  plasmons, and  $F_s$  continues to grow for these high- $k$  plasmons. Enhancement in  $F_s$  for plasmon energies in the retardation region is also apparent.

It should be emphasized again that  $R_c(\hbar\omega)$  in the Mitchell theory should be considered only as an approximation in describing the surface process; the exact strength of the surface effect is not well known. Details of the exact value of  $R_c(\hbar\omega)$ , how-

ever, cannot obscure the physical implications in Eq. (12) and Figs. 6 and 7; namely, the photoyield enhancement for high- $k$  plasmons in the surface theory is enormous and enhancement for low-energy plasmons in this same surface theory also can be large.

If we integrate Eq. (12) over all possible plasmons that can be excited by an excitation of energy  $\hbar\omega$ , the total relative increase in photoyield associated with the volume- and surface-effect photoemissions is given by

$$\frac{\Delta Y(\hbar\omega)}{Y_{\text{vol}}(\hbar\omega)} = \frac{1}{\Delta R(\hbar\omega)} \frac{\sigma^2 \omega^3}{2\pi c^2} \int_0^\infty F(\epsilon_1, \omega_k) [F_v(k) + F_s(k)] \times \frac{k}{P_k} \frac{\gamma_k}{(\omega - \omega_k)^2 + (\frac{1}{2}\gamma_k)^2} g(k) dk. \quad (13)$$

This derivation follows that of Eq. (5). The photoyield predicted in the theories based on volume-plus-surface photoemission effects (assuming a rough surface characterized by a Gaussian autocorrelation function  $\sigma = 15 \text{ \AA}$ ,  $\bar{a} = 450 \text{ \AA}$ ) is plotted in Fig. 3 along with the photoyield from this surface, assuming only the volume theory. Once again, the value for  $Y_c(\hbar\omega)$  or  $R_c(\hbar\omega)$  in the surface theory is the example calculated from Mitchell. It should be noted that a peculiarity of the Gaussian model is that it dies off quite rapidly at high- $k$  values (see Paper I). Thus the relative difference between yields in the surface-plus-volume and only the volume photoeffect is somewhat suppressed near the high- $k$  surface-plasma frequency for this particular roughness model, although the strong enhancement in the surface-effect theory associated with the decay of plasmons excited in the retardation region (lower frequencies) is apparent in Fig. 3. Our experimental results reveal that the actual importance of the surface effect is considerably stronger than indicated in Fig. 3.

### III. EXPERIMENTAL OBSERVATIONS

Three types of experiments were carried out in our photoyield studies. In the first series, highly accurate photoyield measurements were conducted on a series of controlled-roughness Al films to determine the exact magnitude of the roughness-induced yield effects. In the second, both reflectance and photoyield were measured *in situ* on each of a series of roughened Al films to better estimate the photoyield per excited surface plasmon. We believed that this would allow a better understanding of the exact nature of the plasmon-decay process. In the third series, Al photoyield from films of varying roughness was measured as a function of angle-of-light incidence and light polarization. It was hoped that these data would provide (i) information on optical coupling to surface plasmons as a function of light polarization and angle of in-

cidence and (ii) an independent measure of the strength of the surface photoemission effect  $Y_c(\hbar\omega)$  through an analysis of angle-of-light-incidence effects in the photoyield of the smoother Al films.

#### A. High-Accuracy Photoyield Measurements

Photoyield measurements were carried out in standard photoemission chambers.<sup>15,16</sup> Absolute yield values were obtained by comparing our Al yield currents with the currents from a calibrated cesium antimonide (CsSb) tube exposed to the same light beam. Calibration of the CsSb tube has been extensively discussed.<sup>16</sup>

A series of four  $\text{CaF}_2$  overcoated substrates of various coating thicknesses was measured to obtain a wide range of rough surface values; several bowl-feed polished-quartz substrates also were used in an attempt to produce as smooth an Al film as possible. All films deposited on the  $\text{CaF}_2$  overcoated substrates were deposited at  $< 5 \times 10^{-9}$  Torr and 7–10  $\text{\AA}/\text{sec}$ . Results indicated that significant coupling in Al films deposited on bowl-feed polished-quartz substrates still occurred at these evaporation rates and, as a result, the Al deposition rate was raised to 55  $\text{\AA}/\text{sec}$  and the pressure rose to  $8 \times 10^{-9}$  Torr. The deposition of this film was immediately followed by annealing the film at 200–400  $^\circ\text{C}$  for 2 min (see Paper I). This procedure resulted in the smoothest film we have ever measured. Measurements on all films were carried out at  $< 5 \times 10^{-11}$  Torr, and roughness values for Al films on  $\text{CaF}_2$  overcoated substrates were determined as described in Paper I.

The striking results of these studies are presented in Fig. 8. As indicated in Fig. 3, increases in yield on films that are only slightly roughened may be well over 100% greater than our smoothest film photoyield; yield increases in the roughest films are well over an order of magnitude greater than that of the smooth films. One notes that, for even the lowest photoyield curve shown (bowl-feed polished quartz at a deposition rate of 55  $\text{\AA}/\text{sec}$ ), a peak in yield is still evident at the surface-plasma frequency. Some very significant properties of residual coupling in these smooth film samples and a substantiation of our claim that this residual bump is caused by plasma coupling are both discussed in Sec. IV B.

The peaks in yield in Fig. 8 are reasonably well correlated to the surface-plasma frequency, and these peak positions move to lower energies with increased surface roughness just as the reflectance-drop peak positions (Fig. 9, Paper I) move to lower energies for large roughness. One difference between the yield and reflectance peak-energy positions is that the yield peaks lie at systematically higher energies than do the reflectance peaks. This shift to higher energy is consistent

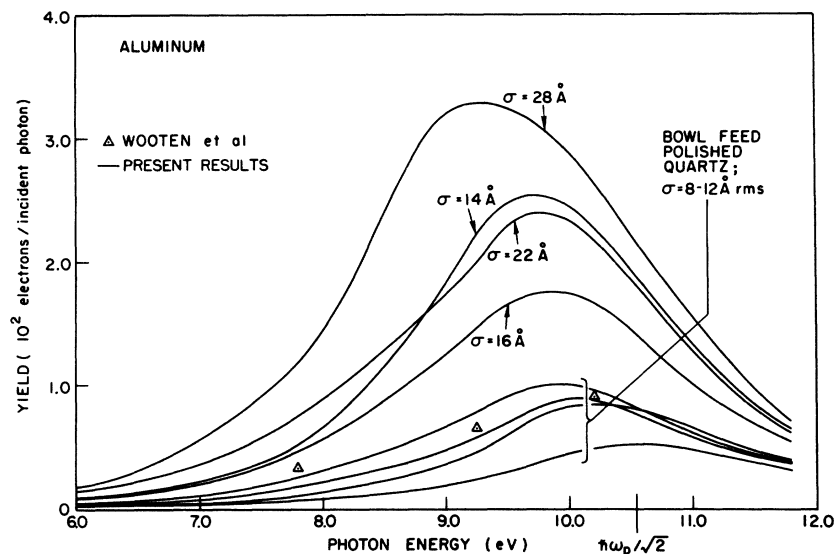


FIG. 8. Al photoyield vs film roughness. The rms roughness values were determined by methods described in Paper I. Also shown (triangles) are Al photoyield values determined by Wooten *et al.*

with the effect that can be associated with the plasmon-field penetration depth enhancement factors of Eqs. (5), (12), and (13) and in Figs. 3, 6, and 7. These factors become quite large as  $\hbar\omega$  approaches  $\hbar\omega_p/\sqrt{2}$  and would be expected to shift the yield peaks to higher energies.

Finally, we note that the increases in yield in these Al curves appear to be well correlated with surface roughness, as is consistent with previous observations in the reflectance of the correlation of plasmon coupling with rms roughness in Ag.<sup>17,18</sup> This occurs despite the strong differences between surface-plasmon coupling in Ag and in Al (see the discussion of surface-roughness spectra accompanying Fig. 6 in Paper I). The one notable exception to the correlation with roughness is the 14-Å roughness curve that indicates extremely strong coupling near the surface-plasma frequency; interestingly, this curve correlates with roughness as it moves to lower energies, and coupling affects the lower surface-roughness  $k$  values. As discussed in Paper I, these low- $k$  surface-momentum components are most strongly correlated to rms roughness, whereas the larger values of the surface momentum (which produce the strong high-energy peak) contribute relatively little to the rms roughness.

#### B. *In Situ* Reflectance and Photoyield Measurements

To better understand the exact mechanism giving rise to the large photoyield effects presented in Fig. 8, it was necessary to measure both photoyield and reflectance on the same rough Al samples. Paper I extensively described how reflectance could be used to determine the roughness spectrum of a surface over a broad spectral range. Such information could be used, in turn, in con-

junction with Eqs. (5) and (13) to evaluate the relative importance of surface- and volume-photoemission effects in explaining observed plasmon-induced yield anomalies in the present studies.

Such reflectance and photoyield measurements were carried out on four Al films of varying roughness; the method used is described by Endriz.<sup>19</sup> It was estimated that these particular reflectance measurements were accurate to  $\pm 2-3\%$ , and the photoyield measurements were accurate to  $\pm 15\%$ . Although the accuracy of these measurements is not particularly impressive, the conclusions implied from the results are so striking that they cannot be altered significantly by errors of even this magnitude.

The results of our reflectance and photoyield measurements are shown in Figs. 9 and 10. In Fig. 9, measurements were made on Al films whose roughness was found to be  $\sigma = 22, 15,$  and  $13 \text{ \AA}$ , respectively. Smooth Al surface-reflectance and photoyield curves are also plotted, as are the computer-calculated theoretical reflectance curves associated with the experimental reflectance-derived surface-roughness spectra (see Paper I).

The derived roughness spectra were used in conjunction with Eqs. (5) and (13) to obtain theoretical expressions for the photoyield increase in both the volume and surface-plus-volume photoexcitation theories. The total calculated photoyield values obtained in these two theories are also shown. A detailed discussion of the implications derived from comparisons of these theoretical and experimental curves can be found in Sec. IV A.

Figure 10 shows the reflectance and photoyield from the smoothest film on which both of these measurements were made. The result is treated separately because reliability of the reflectance

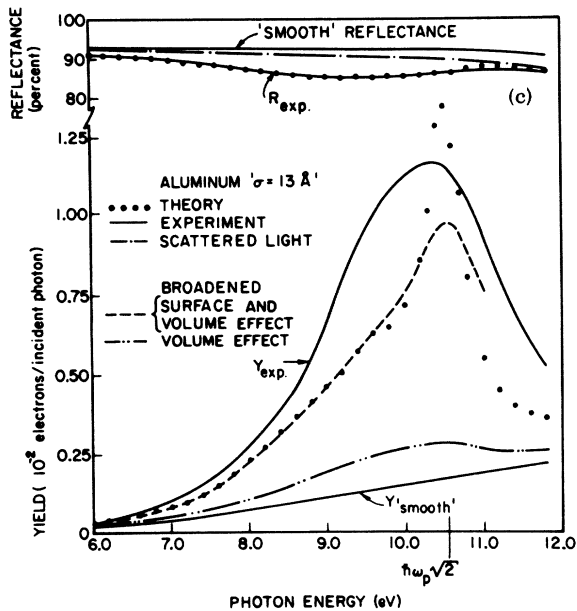
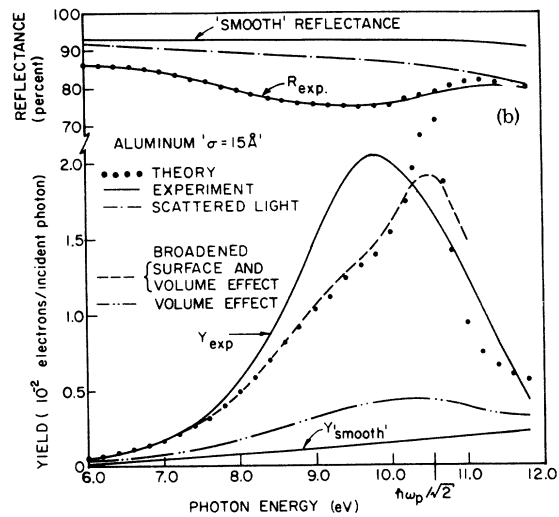
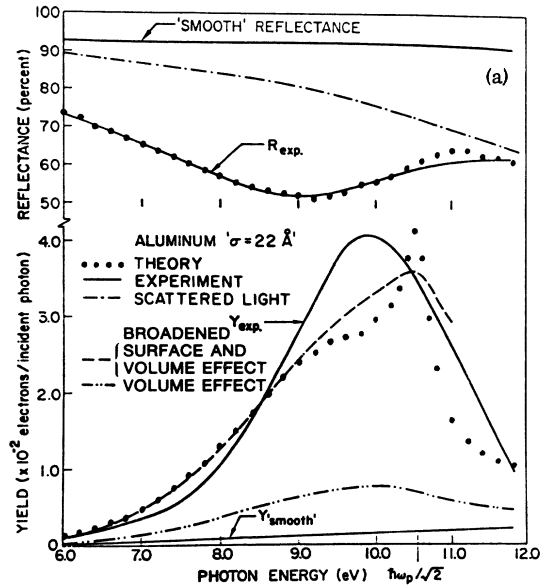


FIG. 9. (a) Reflectance and photoyield for an Al film of  $\sigma = 22 \text{ \AA}$ . The smooth surface Al reflectance and photoyield and the theoretical calculations of the total reflectance drop (dots) and scattered-light-induced reflectance drop (dot-dash) were calculated by the method described in Paper I. The surface-roughness spectrum derived from the reflectance analysis was used with the theory developed in this paper to calculate the total photoyield to be expected in the surface-effect-plus-volume-effect plasmon-decay theory. This calculation is shown as dots. Because the Mitchell model for the surface-effect strength did not yield good agreement with experiment, a single surface-effect strength  $[Y_c(\hbar\omega)]$  was fitted to the results of this experiment and to the results for films shown in Figs. 9(b) and 9(c). Improved agreement with experiment was obtained by using plasmon broadening 2.5 times that predicted by Elson and Ritchie. The photoyield in the pure volume-effect theory for the plasmon decay (with 2.5 times normal broadening) emphasizes the inability of the volume theory to explain the experimental results. (b) Reflectance and photoyield for an Al film of  $\sigma = 15 \text{ \AA}$ . Optical reflectance measurements were used to determine the roughness spectrum which was, in turn, used to generate theoretical expressions for the photoyield in the volume-effect and the volume-plus-surface-effect plasmon-decay theories. (c) Reflectance and photoyield for an Al film of  $\sigma = 13 \text{ \AA}$ .

is questioned in this smooth surface limit. As a consequence, only the photoyield was plotted. The measured reflectance fell approximately 1% below the more highly accurate "smooth" surface reflectance over most of the spectral range. However, it was believed that plotting this reflectance would be somewhat misleading because the error brackets are considerably larger than all reflectance differences of interest in the figure. Instead, we plotted only the "smooth" reflectance and error

brackets indicating the range of possible reflectance values for the film. (Reflectance was measured each 0.2 eV, but error brackets have been plotted at four points only because of the lack of variation in the measured reflectance.) Also plotted are theoretical reflectance and photoyield, assuming an analytical surface-roughness function discussed in Sec. IV. This function was assumed because the reflectance measurements could not be used to determine reliably the actual roughness

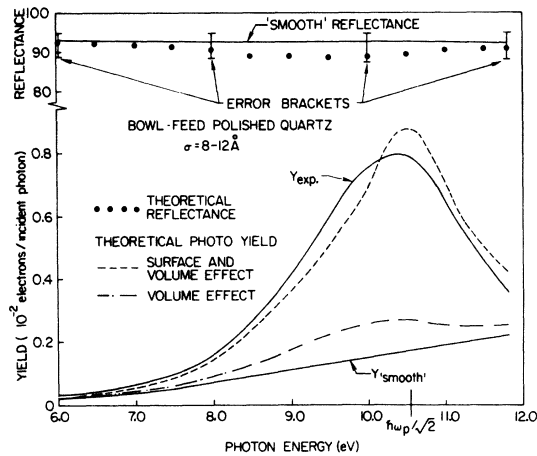


FIG. 10. Smoothest sample on which both reflectance and photoyield measurements were made. The difference between measured reflectance and smooth surface reflectance was too small to allow the determination of the roughness spectrum; consequently, only the error brackets signifying the possible range of reflectance values are plotted. The theoretical photoyield curves in the volume-effect theory and in the volume- plus surface-effect theory were calculated, assuming (i) an analytic "stepped" surface-roughness function, (ii) 2.5 times normal plasmon broadening, and (iii) the characteristic surface-effect strength  $[Y_c(\hbar\omega)]$  determined from the match to the results in Figs. 9(a)–9(c). The associated theoretical reflectance for this roughness model (dotted curve) lies within error brackets of the measured reflectance.

spectrum, as was done for the films in Fig. 9.

### C. Photoyield vs Polarization and Angle-of-Light Incidence

Photoyield was measured as a function of light polarization and angle of incidence to gain information from the rougher films concerning the dependence of optical coupling to surface plasmons on these two parameters. In the smoother films, it

was hoped that data would be obtained regarding the strength of the surface-effect photoemission so that an independent experimental check of this effect might be carried out.

The measurements were made using a uv polarizer designed and constructed by Derbenwick.<sup>20</sup> Angle-of-light incidence was varied, employing the same apparatus as was used to make the reflectance and photoyield measurements described in Sec. III B, and by a method discussed by Endriz.<sup>19</sup>

The  $\sigma = 15$  and  $13 \text{ \AA}$  and the smooth Al films whose near-normal ( $8^\circ$ ) angle-of-light-incidence photoyield are seen in Figs. 9 and 10 were also the films investigated vs angle-of-light incidence and light polarization. The results of these studies are shown in Figs. 11 and 12. In Fig. 11, the ratios of photoyield measured at an angle-of-light incidence of  $34.5^\circ$  vs the photoyield measured at an angle-of-light incidence of  $8^\circ$  are plotted. (Throughout these experiments, a light beam whose half-angle was less than  $1.5^\circ$  was used, so that the actual angles cited should be considered averages of a light cone whose full width is somewhat less than  $3^\circ$ .) Measurements were made on both the S (perpendicular to the plane of incidence) and P (parallel to the plane of incidence) polarizations for each of the three films. Also shown are the ratios for  $[1 - R_s(\theta)]\alpha(\theta)$  and  $[1 - R_p(\theta)]\alpha(\theta)$ , calculated from the Al optical constants and related to the photoyield in the volume-effect theory discussed in Secs. II and IV.

In Fig. 12, we see plots of the ratio of photoyield vs angle-of-light incidence normalized to the photoyield at  $8^\circ$  incidence. The plots in Fig. 12(a) are for an excitation frequency of 7.8 eV (far removed from the high- $k$  surface-plasmon frequency), and the plots of Fig. 12(b) are for an excitation frequency of 10.2 eV (quite near the high- $k$  plasmon frequency). Again, measurements were made on both the S and P polarizations.

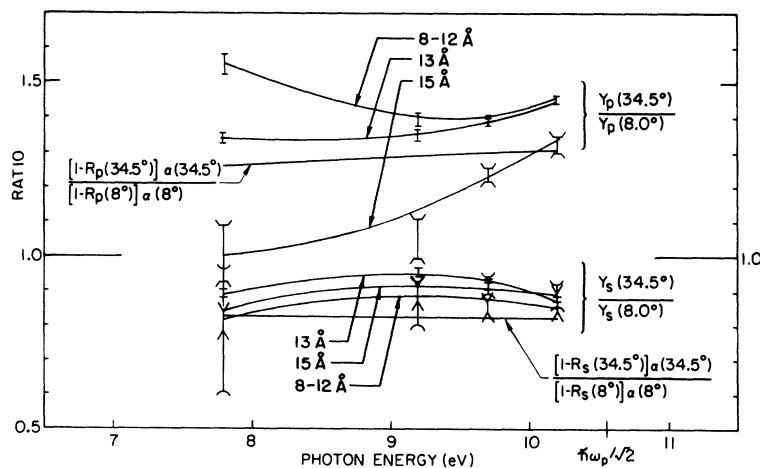


FIG. 11. Photoyield vs angle-of-light incidence. Shown are the ratios of photoyield at angle-of-light incidence ( $34.5^\circ$ ) to photoyield at near-normal incidence ( $8^\circ$ ), for both s- and p-polarized light and photon-excitation energies of 7.8, 9.2, 9.7, and 10.2 eV. Films of three roughness values are plotted, as are the ratios of  $[1 - R_p(\theta)]\alpha(\theta)$  and  $[1 - R_s(\theta)]\alpha(\theta)$  at  $34.5^\circ$  to these same parameters calculated for  $\theta = 8^\circ$ . These latter ratios were calculated from Al optical constants derived in Paper I and are equal to the relative change in photoyield vs angle in the volume-effect photoemission theory.

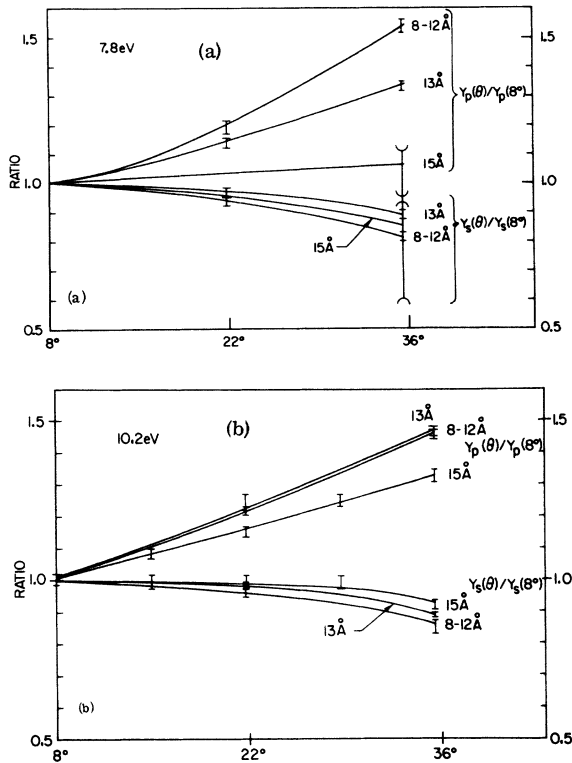


FIG. 12. (a) Photoyield vs angle-of-light incidence for an excitation energy of 7.8 eV. Shown are the ratios of photoyield at a given angle-of-light incidence to photoyield at near-normal incidence ( $8^\circ$ ) for both  $s$ - and  $p$ -polarized light. Curves are plotted for three different films. (b) Photoyield vs angle-of-light incidence for excitation energy 10.2 eV. Shown are the ratios of photoyield at a given angle-of-light incidence to photoyield at near-normal incidence ( $8^\circ$ ) for both  $s$ - and  $p$ -polarized light. Curves are plotted for three different films.

Because use of a polarizer introduces an enormous attenuation in the strength of our light signal,<sup>20</sup> photoyield could only be measured at the spectral points indicated in Fig. 11, where the strength of our light source was appreciable. Even at these excitation frequencies, the uncertainty in our measurements was quite significant, as indicated by the error bars in Figs. 11 and 12.

Any interpretation of our photoyield data should be tempered by the magnitude of these error brackets; nevertheless, a few points are clear despite these accuracy constraints. First, in the film described in Fig. 9(b), the roughness-induced photoyield increase is much greater than the smooth surface photoyield over the spectral range studied. This would appear to indicate that the surface-plasmon-related photoyield process dominates the photoyield from the  $\sigma = 15 \text{ \AA}$  film over virtually the entire spectral range. In fact, we note from Figs. 9(b), 9(c), and 10 that the photo-

yield at 10.2 eV is dominated by the plasmon process in all three films. The polarization and angle-of-light-incidence effects, therefore, should be related directly to the dependence of surface-plasmon coupling on these parameters for the 15- $\text{\AA}$  film over its entire spectral range and for the smoother films at energies approaching their surface-plasma frequency. It is interesting to note that the angle of  $p$  polarized light incidence curves for 10.2 eV is relatively insensitive to film roughness, which would appear to support the interpretation that the plasmon-decay process dominates the yield of all three films at 10.2 eV. (A common plasmon-decay process is giving rise to angle-of-light-incidence photoyield effects at 10.2 eV and these angle effects are insensitive to the magnitude of the roughness when the roughness reaches a critical value for which plasmon decay dominates the photoyield.) The 10.2 eV curves might be thought of as indicating the angular dependence of coupling to surface plasmons. In Fig. 11, it may not be unreasonable to take the curves over the entire frequency range for the relatively rough 15- $\text{\AA}$  film as the angular dependence of coupling to plasmons. These curves would seem to indicate that the angular dependence of coupling to plasmons in the retardation region of 7.8 eV (see Fig. 1, Paper I) is not as great as the dependence in the high- $k$  region of 10.2 eV.

The second observation from the results in Figs. 11 and 12 is that differences between films in the dependence of photoyield on angle of  $p$  polarized light incidence become large at 7.8 eV. This dependence is strongest in the smoothest film and, as seen in Fig. 10, coupling to plasmons is reasonably small at 7.8 eV in those particular films. These observations strongly suggest that the mechanism giving rise to the angle-of-light-incidence effect in the smoothest film is distinct from the mechanism giving rise to this effect in the rougher films. In Sec. IV, we postulate that the strong angle-of-light-incidence-dependent surface photoeffect is significant in explaining the observed photoyield at 7.8 eV. It should be realized that this assumed mechanism is a direct surface photoexcitation, does not require the intermediate plasmon excitation, and can occur at off-normal incidence on even perfectly smooth surfaces. The implication that the surface photoeffect also manifests itself in this independent measurement in which plasmon excitation plays a minor part indicates that the smooth film measurement at 7.8 eV may be used to independently determine the characteristic strength  $Y_c$  of the surface photoeffect.

#### IV. DATA ANALYSIS AND DISCUSSION

It is evident from the results in Figs. 8 and 9 that the roughness-induced photoyield effect is ex-

tremely sensitive to surface roughness and is strongly correlated to the surface-plasmon frequency. In the discussion that follows, we are concerned with the details of the plasmon-decay mechanism which gives rise to these photoyield effects. Attempts are made to explain the results with a model based on the volume-photoemission effect and with one based on the surface effect. The extreme sensitivity that the effect has on surface roughness is reexamined. Additional experimental data are presented to indicate that photoyield provides a practical means of monitoring annealing effects in Al films, and evidence is presented to prove that roughness-induced photoyield increases are virtually impossible to eliminate in vacuum-evaporated Al films.

#### A. Volume vs Surface Photoemission Effects

In Sec. II, theoretical expressions for the increase in photoyield were derived from rough surfaces characterized by arbitrary roughness spectra  $g(k)$ . Equation (5) expressed this increase, assuming that the plasmon decay photoexcites electrons primarily in the volume theory of photoemission. In Eq. (13), a comparable expression includes contributions to the photoyield in both the volume- and surface-effect theories.

Photoyield increases in the volume theory are determined by the Al optical constants (Paper I), the smooth surface Al photoyield and reflectance, the electron escape depth  $l$ , and the surface-roughness spectrum  $g(k)$ . Al smooth surface reflectance was first measured by Feuerbacher and Steinman<sup>21</sup> and was confirmed by our measurements in Paper I. Smooth surface Al photoyield and electron-escape depth are estimated in Sec. IV B. The only variable parameter in the volume-effect theory is the roughness spectrum  $g(k)$ . This is in contrast with Eq. (13) which is in terms of the unknown surface-effect strength  $Y_c(\hbar\omega)$  as well as the surface roughness spectrum  $g(k)$ .

It is apparent, therefore, that, although a direct verification of the theory that includes the surface effect is obscured by our imperfect knowledge of the strength of  $Y_c(\hbar\omega)$ , a direct check on the ability of the volume-effect theory to explain observed photoyield is possible. In Fig. 9, reflectance and photoyield were measured on the same sample. The reflectance measurement indicates the number of photons that are scattered and absorbed from the incident beam, and the method of analysis (Paper I) yields the surface-roughness spectrum  $g(k)$ , along with the relative number of photons that are scattered out of the incident beam and absorbed by surface oscillations. The theoretical reflectance calculated from these derived spectra, including both scattering and surface-plasmon-induced effects, is plotted in Fig. 9.

#### 1. Superiority of Surface-Effect Theory

The roughness spectra derived for the samples described in Fig. 9 were employed to calculate the theoretical photoyield in the volume-effect theory [Eq. (5)]. The results indicate the total inability of the volume-effect theory to explain the magnitude of the observed plasmon-induced photoyield effect. It should be noted that a lifetime broadening 2.5 times that predicted in Elson and Ritchie's theory was used, but this additional broadening did not appreciably affect the shape or magnitude of the "volume" curve; it was included so that the calculation would be consistent with the additional broadening used in the surface-effect calculations. In all three samples described in Fig. 9, the yield calculated in the pure volume-effect theory accounted for less than  $\frac{1}{4}$  of the rough surface increase in photoyield near the surface-plasma frequency and was even less able to explain the increase in rough surface photoyield occurring at lower energies.

The derived roughness spectra for the films in Fig. 9 were used also to calculate the increase in photoyield that would occur if both volume- and surface-photoemission effects were of importance [Eq. (13)], and these results also are shown in Fig. 9. Calculations in the normal broadening predicted within the Elson-Ritchie theory are represented by dots, broadened by an additional factor of 2.5 represented by dashed curves. A single-surface photoemission-effect strength  $Y_c(\hbar\omega)$  was fitted to experiment for all three samples and obtained consistent results. The magnitude of that surface-effect strength is compared (Fig. 13) to the surface-effect strength as calculated in Mitchell's theory, assuming a step surface-potential discontinuity; also shown is our estimate of smooth surface Al photoyield as determined in Sec. IV B. Although noticeably greater at higher energies than the value predicted in the Mitchell model, our assumed surface-effect photoyield is not so different as to be unreasonable. It should be noted that the accuracy of the derived magnitude of  $Y_c(\hbar\omega)$  is somewhat less than the  $\pm 15\%$  accuracy of the photoyield data used in calculating  $Y_c(\hbar\omega)$ .

Returning to the detailed analysis of the theoretical and experimental photoyield curves in Fig. 9, note that the surface-effect curves calculated with normal broadening are not in particularly good agreement with experiment. The normal-broadening curve reveals an extremely sharp photoyield peak at the surface-plasma frequency, which is associated with the strong photoyield enhancement that occurs in the surface-effect theory for high- $k$  plasmons (see Figs. 6 and 7). The introduction of additional broadening was motivated not only by the improved agreement, but also because of the

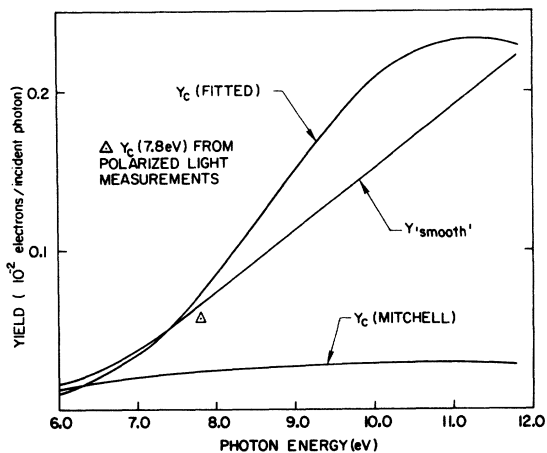


FIG. 13. Experimentally determined surface-effect strength  $Y_c(\hbar\omega)$ . Shown is  $Y_c$  (fitted) as determined from a fit of our plasmon-decay theory to the experimental plasmon-induced photoyield increases shown in Figs. 9(a)–9(c). Also shown for comparison is the value for  $Y_c$  (7.8 eV) determined independently from polarized light measurements (triangle),  $Y_c$  determined by Mitchell, and the Al smooth surface photoyield.

indications in the reflectance data of Paper I, and particularly in the extremely smooth surface photoyield effects shown and discussed in Sec. IV B, that the normal broadening in the Elson-Ritchie theory simply is not large enough to explain any of the observed broadening. An increased broadening factor of 2.5 was derived from the fit of theory to experimentally observed “smoothest” surface Al photoyield as discussed in Sec. IV B.

Even with the improved agreement between the experiments in Fig. 9 and the broadened surface-effect theory, a noted difference in the peak positions still appears in the photoyield. The theoretical peak positions continue to lie very close to the high- $k$  plasma frequency, which is considerably higher than the experimental peak positions. This is again an artifact of the strong enhancement of photoyield from high- $k$  plasmons, which occurs in the surface-effect theory. The photoyield will occur at the high- $k$  plasmon frequency if the surface effect is included. This would imply that, if the surface-effect theory is important in explaining our data, the assumption made throughout the theoretical developments of Ritchie and others that the plasmon eigenfrequencies are unperturbed by the rough surface may be incorrect. The curves in Fig. 9 suggest that the shift of the photoyield peak to lower energies may be associated with a shift of the high- $k$  plasmon eigenfrequencies to slightly lowered energy. This assumption varies fundamentally from the interpretations in Paper I and the theoretical calculations in Fig. 9. These interpretations assumed that shifts in coupling to

surface plasmons to lower energies were the result primarily of variations in the roughness spectra which caused coupling to plasmons further down in the retardation region but that the plasmon eigenfrequencies were unperturbed by the surface geometry. Our interpretation is more consistent with the earlier assumptions that plasmon excitations at lower energies were caused by strong geometrical effects on the surface. It has been suggested, for example, that hemispherical surface bumps would have associated frequencies of  $\hbar\omega_p/\sqrt{3}$  rather than the  $\hbar\omega_p/\sqrt{2}$  for the smooth surface. These two distinct approaches to optical excitation of surface polarization charge are not mutually exclusive and, even if a roughness-induced perturbation of the plasmon eigenfrequency is significant, both processes might occur simultaneously in the surfaces.

Despite the differences in the details of the experimental curves (Fig. 9) and the theoretical curves based on surface-effect photoemission, the surface-effect theory is in superior agreement with experiment than is the volume theory. Because an arbitrary surface-effect strength was assumed, this agreement does not strongly imply that the surface effect is important in describing the plasmon-decay process. There are, however, several contributing arguments and additional experimental evidence that tend to support this conclusion. The total inability of the volume theory to explain experimental results is again reemphasized. The volume theory is well defined and the expected error in this calculation is quite small. The surface-effect interpretation is strengthened by the failure of the volume theory because it is virtually the only alternative mechanism that can reasonably describe the plasmon-decay process. We have considered<sup>19</sup> the possibility of photoyield enhancement associated with a roughness-induced increased escape probability, but this process has been rejected because such effects are expected to be associated with the mean surface slope which, for even the roughest surfaces, provides only a small perturbation on the smooth surface escape function. Other possible mechanisms have been proposed and rejected.

The surface-effect theory also is strengthened by its applicability over a broad range of roughened surfaces. In addition to the agreement shown for the three surfaces in Fig. 9, we see in the measurements of a fourth surface (Fig. 10) an attempt to match the surface-effect theory to experiment by assuming an analytical surface-roughness function. This function was Gaussian, characterized by  $\sigma = 8 \text{ \AA}$ ,  $\bar{a} = 450 \text{ \AA}$ , and a “stepped roughness” function described in Sec. IV B and characterized by a mean stepping distance of  $\sim 70 \text{ \AA}$ . The significant aspect of this calculation is that the as-

sociated reflectance for this model lies within the error brackets of the measured reflectance. (This is not a particularly satisfying criterion but is probably as far as one can extend an interpretation of the rather poor reflectance data taken on the sample described in Fig. 10.) As an additional factor supporting our surface-photoeffect approach, we note in Sec. IV B that the derived strength of  $Y_c(\hbar\omega)$  is quite successful in explaining observed photoyield in even our smoothest Al film.

As a final and extremely important point, the polarized light measurements provide an independent estimate of the strength of  $Y_c(\hbar\omega)$  at 7.8 eV. At this frequency, the "smooth" surface photoyield for the  $\sigma = 8-12 \text{ \AA}$  film accounts for an appreciable amount of the total photoyield at near-normal ( $8^\circ$ ) angle-of-light incidence. This photoyield at  $\theta = 8^\circ$  can be expressed as

$$Y(7.8 \text{ eV}, \theta = 8^\circ) = Y_{sp}(7.8 \text{ eV}, \theta = 8^\circ) + Y_{smooth}(7.8 \text{ eV}, \theta = 8^\circ), \quad (14)$$

where the yield contribution from surface plasmons  $Y_{sp}$  and from the normal photoexcitation process  $Y_{smooth}$  can be found in Fig. 10. At an angle of incidence of  $8^\circ$ , the contribution to  $Y_{smooth}$  can be assumed to come primarily from the volume-effect photoemission; at higher angles of incidence, the discussion in Sec. II implies that the photoyield will also include a surface-effect component and will be given for  $p$ -polarized light by

$$Y_{smooth, p}(7.8 \text{ eV}, \theta) = Y_{smooth, p, vol}(7.8 \text{ eV}, \theta) + Y_{smooth, p, surface}(7.8 \text{ eV}, \theta). \quad (15)$$

The first of these terms can be shown to vary with  $\theta$  as

$$\{[1 - R_p(\theta)] \alpha(\theta) / [1 - R_p(0)] \alpha(0)\} \times Y_{smooth}(7.8 \text{ eV}, \theta = 0)$$

for  $p$ -polarized light, and we can assume

$$Y_{smooth, vol}(7.8 \text{ eV}, \theta = 0) \cong Y_{smooth, vol}(7.8 \text{ eV}, \theta = 8^\circ).$$

The second term can be shown to vary with  $\theta$  as

$$\{[|\vec{a}_{st} + \vec{a}_{sr}|^2 / |\vec{a}_t|^2] Y_c(7.8 \text{ eV})$$

[Eq. (6)] for  $p$ -polarized light. If the variation with  $\theta$  of  $Y_{sp}(7.8 \text{ eV}, \theta)$  is assumed to be well approximated by the  $\sigma = 15 \text{ \AA}$  curve for  $p$ -polarized light in Fig. 12(a), the inclusion of the surface effect in the expression for the angular dependence of the total photoyield from  $p$ -polarized light,

$$Y_p(7.8 \text{ eV}, \theta) = Y_{sp, p}(7.8 \text{ eV}, \theta)$$

$$+ Y_{smooth, p}(7.8 \text{ eV}, \theta), \quad (16)$$

yields an expression uniquely and completely defined by the Al optical constants, existing experimental data in Figs. 10-12(a), and the unknown surface-effect strength parameter  $Y_c(7.8 \text{ eV})$ .

In Eq. (16),  $Y_c(7.8 \text{ eV})$  was varied so as to agree with the experimentally observed photoyield for  $p$ -polarized light incident at  $34.5^\circ$  on the  $\sigma = 8-12 \text{ \AA}$  film. The errors in the parameters used in this calculation were noted, and values were chosen within the error brackets so as to minimize the derived value of  $Y_c$ . The value found for  $Y_c(7.8 \text{ eV})$  was  $\approx 0.9$  times the smooth surface photoyield at 7.8 eV and  $\approx 2.4$  times the value calculated in Mitchell's assumption of a step surface-potential discontinuity. This derived value is shown as a triangle at 7.8 eV in Fig. 13 and is in excellent agreement with the value for  $Y_c(7.8 \text{ eV})$  derived independently from our match of the surface-photoeffect theory to the experimentally observed plasmon-induced photoyield increases described in Fig. 9.

In summary, the photoyield for 7.8-eV  $p$  polarized light increases by a factor of  $\approx 1.6$  as the angle-of-light incidence is increased from  $8^\circ$  to  $34.5^\circ$  on our smoothest film. The increase in

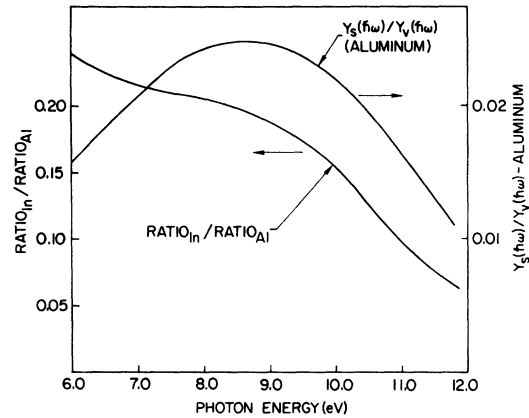


FIG. 14. Surface-effect-to-volume-effect photoemission ratios. Shown is the ratio of surface-effect-to-volume-effect photoemission  $Y_s(\hbar\omega)/Y_v(\hbar\omega)$  expected from an ideal film, assuming the characteristic surface-effect strength derived from experiment and plotted in Fig. 13 and assuming optical excitation at normal incidence by an unpolarized light cone of a half-angle of  $10^\circ$ . Also shown is a plot of the ratio of the factor

$$\frac{|\vec{a}_{st} + \vec{a}_{sr}|^2}{|\vec{a}_t|^2} \frac{1 + \alpha(\theta)l}{\alpha(\theta)l\Delta R(\theta, \hbar\omega)}$$

evaluated for indium to the value of this same factor evaluated for Al. This ratio yields a measure of the importance of the surface relative to the volume photoeffect. Thus, the relative surface-effect strength will be approximately 20% as strong in In as in Al.

yield over this angular range for our roughest film (in which plasmon decay dominates the photoyield) was negligible, indicating that the optical coupling to plasmons must be relatively insensitive to angle at an excitation energy of 7.8 eV. Calculations indicated that yield in the "volume" -photoeffect theory should not be as sensitive to angle of incidence. The conclusion is that the surface-photoemission effect appears to be the only mechanism capable of explaining the strong angular dependence at 7.8 eV for the photoyield of the smoothest film on which this angle-of-light-incidence measurement could be made.

Despite some disagreement between our experimental results and theoretical calculations, the over-all agreement between theory and experiment and the strong agreement between  $Y_c(7.8 \text{ eV})$  as determined from the plasmon-induced photoyield increases and as determined from our polarized-light measurements indicate that surface-effect photoemission can be a significant process in photoemission from Al. Results reveal that the surface effect dominates the photoemissive process associated with the decay of optically excited surface plasmons. This experimental evidence is believed to be the strongest evidence to date for the existence of this historically important surface photoemission effect.

## 2. Limitations of the Surface-Effect Theory in Photoemission Experiments

The conclusion reached in the above Sec. IV A 1 that the surface-effect photoemission is the dominant source of photoyield in the decay of surface plasmons could be misleading in view of the volume-effect interpretation of photoyield measurements over recent years, and this conclusion should be placed in perspective. The surface plasmon has some very unique properties relating to field polarization and energy penetration into the medium (Sec. II), and these result in a strong enhancement of the surface-effect photoexcitation process. In addition, Al is also unique and probably one of the best examples of a "Sommerfeld model" for a metal. It is not surprising, therefore, that the plasmon-induced surface effect is so strong in Al.

In most photoemission experiments and in virtually all our previous photoemission experiments, near-normal angle-of-light incidence is employed. The half-angle of divergence for the light beams is usually less than  $10^\circ$ . It can be seen in Fig. 4 that the quadratic dependence of the surface effect on angle-of-light incidence results in considerable suppression of the surface effect for a light beam incident on a perfectly smooth surface at such small angles. Since our light sources are unpolarized and since a light cone or half-angle  $\theta_c$  actually

has a mean angle considerably less than  $\theta_c$ , an additional suppression of the surface effect occurs. If the ratio of surface-effect-to-volume-effect photoemissions from a perfectly smooth surface of Al is calculated assuming an unpolarized incident light cone of half-angle  $10^\circ$  and the surface-effect strength  $Y_c(\hbar\omega)$  derived from our plasmon-decay measurements and plotted in Fig. 13, the result obtained will be as seen in Fig. 14.

Here, the surface effect is less than 3% of the volume effect over the entire spectral range. This occurs in a metal whose surface-effect strength is apparently strong enough so that it will be equal to or greater than the volume effect for  $p$  polarized light incident at angles larger than  $45^\circ$ . The suppression of the surface effect in a typical photoemission experiment is purely a classical optical effect, and it is surprising that so little attention has been given to this factor. It might appear that, in the present studies of rough surfaces, surface roughness would provide an alternate channel for field components normal to the surface (ignoring the plasmon effect) even with near-normal-incidence light; however, measurements<sup>1</sup> have tended to indicate that real surfaces are characterized by autocorrelation lengths in the range 500–1000 Å. Because the mean surface slope is related to the ratio  $\sigma/\bar{a}$  (the mean slope for a Gaussian surface-roughness model is given<sup>22</sup> by  $\sqrt{2}\sigma/\bar{a}$ ), the mean slope for even our roughest films is probably not large enough to contribute any more to the surface effect than is contributed by the divergence of the normally incident light beam. For example, the mean surface slope in a film for which  $\sigma = 25 \text{ Å}$  would be a mere 0.07 rad if one assumed a Gaussian autocorrelation function and an autocorrelation length of 500 Å.

Because Al is an exceptionally good approximation to the free-electron metal, its surface-to-volume photoeffect would be expected to be appreciably stronger than the effect in other metals. The expression in Eq. (9) provides a particularly useful means of comparing the relative strengths of the surface-to-volume-photoemission-effect ratios for various metals and, in Fig. 14, the ratio of surface-to-volume photoemissions for Al and In has been compared. Indium is considered a fairly good nearly free-electron metal and, because it is trivalent, its plasma frequency and Fermi energy are not much different from Al. Because its work function is also comparable to Al, the second factor in Eq. (9) should not vary that much between the two metals and, therefore, only the first factor

$$\frac{|\vec{a}_{s1} + \vec{a}_{sp}|^2}{|\vec{a}_t|^2} \frac{1 + \alpha(\theta)l}{\alpha(\theta)l \Delta R(\theta, \hbar\omega)}$$

is plotted in Fig. 14. The In optical constants and the value used for  $l$  in indium (50 Å) were ob-

tained from Koyama,<sup>23</sup> and the results (Fig. 14) confirm our suspicion that the surface-to-volume photoemission effect would be smaller in metals other than Al. It would be of value of pursue the calculations in Eq. (9) for other metals to determine in which metals one would most easily see the surface-photoemission effect.

It can be concluded, therefore, that, in metals or at frequencies for which the extremely strong plasmon-induced surface photoeffect can be ignored, there is very little chance to observe surface-effect photoemission with near-normal incidence light on reasonably smooth surfaces, even in a free-electron metal such as Al.

#### B. High Sensitivity of Photoyield to Surface-Plasmon Decay

The high sensitivity of Al photoyield to plasmon decay allows it to be used as a very sensitive measure of surface roughness. The sensitivity of this yield is so strong that the photoyield increase near the high- $k$  surface-plasma frequency (10.55 eV) was virtually impossible to eliminate in even our smoothest vacuum-evaporated Al films. In Sec. IV B1, we present the lowest experimental photoyield that we were able to observe on our "smoothest" Al films. Our method was to estimate the Al smooth surface photoyield, and this approach will be described and justified. The discussion of  $Y_{\text{smooth}}$  is followed in Sec. IV B2 by an attempt to explain the residual-roughness photoyield effects in our smoothest Al films in terms of a surface-roughness model that includes the discrete stepping of the surface which occurs in real metals having finite lattice constants. In Sec. IV B3 further experimental data are presented to indicate that this highly sensitive roughness-induced photoyield effect provides an extremely powerful tool for monitoring annealing effects in Al films.

##### 1. Smooth Surface Photoyield

Our lowest photoyield Al samples were obtained by rapidly evaporating Al on bowl-feed polished-quartz substrates and following with a 200–400 °C annealing of the film for 1–2 min. This annealing process tended to substantially "smooth" our films. Even with these rather complex preparation procedures, we were unable to eliminate residual-roughness effects on the photoyield at the high- $k$  plasmon frequency. Measurements on two such films showing the lowest photoyield that we obtained are plotted in Fig. 15; note that they are an order of magnitude lower than the largest yields (see Fig. 8).

Much of the interpretation in Sec. IV A depended on knowledge of the photoyield expected from a perfectly smooth Al surface. Our failure to obtain this information forced us to estimate its value

from the results in Fig. 15 (the estimated curve labeled  $Y_{\text{smooth}}$ ). The immediate question is whether the experimental results shown in Fig. 15 might actually be the smooth surface Al photoyield; that is, is it possible that the smooth surface Al photoyield actually has a peak near 10.5 eV, which is intrinsic to the metal itself? The answer is probably no. The peak position for our smoothest film is within less than 0.05 eV of the value of  $\hbar\omega_p/\sqrt{2}$  obtained from the experimental value for the volume-plasma frequency. This correlation of peak position to the surface-plasma frequency is far too close for coincidence. To double check whether this peak might be intrinsic to the material, a very crude first-order theoretical calculation of the photoyield expected from smooth Al was carried out. It assumed that the internal distribution of photoexcited electrons, at excitation energy  $E$ , well approximated the density of filled states in Al at  $E - \hbar\omega$ . The calculation further assumed that the relative total number of electrons excited was proportional to  $1 - R(\hbar\omega)$ , that the fraction of electrons reaching the surface was proportional to  $\alpha(\hbar\omega)l$  (the electron escape depth  $l$  was assumed constant), and that the classical escape-probability function could be used (see Sec. II). The results indicated that the smooth surface Al photoyield should be an almost linear monotonically increasing function over the entire 6.0–12.0 eV spectral range.

With this justification, the smooth surface Al photoyield was estimated by linearly extrapolating the low-energy photoyield of our smoothest film in the manner indicated in Fig. 15. In addition to providing the values for  $Y_{\text{smooth}}$  this new estimate provided improved yield data for the calculation of the electron inelastic scattering length (escape depth) in Al. It was noted (Fig. 8) that Wooten *et al.*<sup>24</sup> had carried out photoyield measurements in Al and obtained results that indicated appreciable

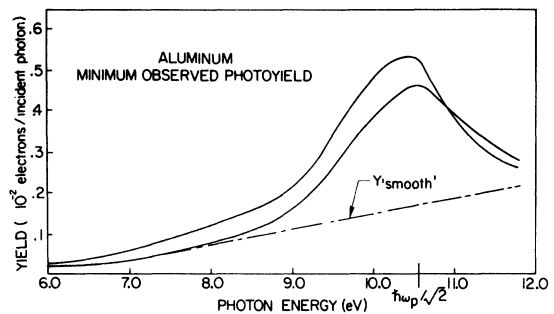


FIG. 15. Minimum observed Al photoyield. Shown are the two lowest photoyield measurements made on Al for two extremely smooth films. Also shown is our estimate of the ideal smooth surface photoyield obtained by linearly extrapolating the low-energy photoyield of the smoothest film.

surface-plasmon coupling. Wooten had matched Monte Carlo calculations of the electron transport-escape probability to his experimental photoyield to estimate electron inelastic scattering lengths. His results yielded scattering lengths that were large in comparison to similar calculations of other metals<sup>25,26</sup>; he has since recalculated these electron inelastic scattering lengths,<sup>27</sup> using what we believe to be an improved estimate of Al photoyield shown in Fig. 15, and his new results appear to be considerably more reasonable than previous values. The constant value of  $l = 70 \text{ \AA}$ , used throughout the calculations in this paper, is equal roughly to the inelastic scattering length for an electron 10.0 eV above the Fermi level, as found in the most recent calculations by Wooten.

## 2. "Residual-Roughness" Photoyield

The strong coupling to plasmons observed in photoyield from even our smoothest films is in marked contrast with the rather weak coupling observed in reflectance of smooth Al films. It was noted by Feuerbacher and Steinman<sup>21</sup> and confirmed in our reflectance studies that the residual-roughness effect could be reduced to less than 1%. Although no reflectance data were available for the smoothest samples on which highly accurate photoyield measurements were taken, these independent smooth surface reflectance measurements would strongly indicate that the reflectance drop associated with the photoyield peaks of Fig. 15 should be approximately 1%.

If the photoyield per decaying plasmon is calculated from the yield increase and the estimated reflectance drop in this smooth film case, a value of  $\approx 0.3$  electrons (decaying plasmon)<sup>28</sup> can be obtained. This is greater than even the strong enhancement observed in the films described in Figs. 9 and 10. The strong enhancement and occurrence of the photoyield peak in these smooth surfaces at the high- $k$  surface-plasma frequency combine to suggest that the effect is associated with the excitation of very-high- $k$  plasmons. It was apparent (Fig. 6) that an enormous enhancement in photoyield per excited plasmon occurs for such high- $k$  plasmons.

None of the standard mathematical models for surface roughness (Lorentzian, exponential, Gaussian) can explain the presence of such high- $k$  roughness components in smooth surfaces, assuming reasonable autocorrelation lengths ( $\bar{a} = 100\text{--}1000 \text{ \AA}$ ). This, in turn, motivated us to reexamine the nature of very smooth vacuum evaporated films and to attempt to derive a general surface-roughness model which could be used to describe these surfaces.

(a) *Surface-roughness stepping function.* The presence of high- $k$  spectral components suggested

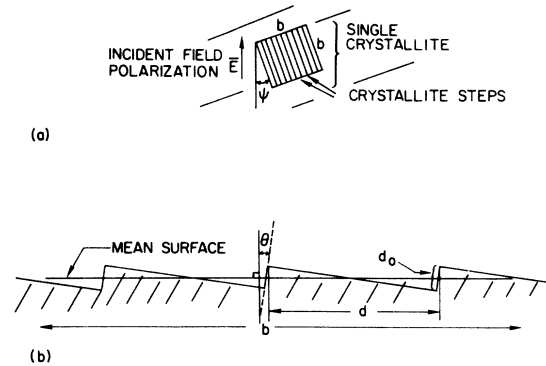


FIG. 16. Stepped-roughness model showing (a) a top view of one of the square crystallites of arbitrary dimensions  $b \times b$ ,  $b \gg d$ , where  $d$  is the distance between parallel surface-height steps of magnitude  $d_0$ , and (b) a side view of the surface-height variation.

sharp discontinuities in the surface, and the very low rms roughness of our smoothest films ( $\sigma < 10 \text{ \AA}$ ) suggested that the discrete stepping of the crystal associated with a finite lattice constant ( $d_0 = 4.1 \text{ \AA}$  for Al) could be important. Clearly, the stepping or terracing of the smooth surface provides the exact type of high- $k$  spectral components required to explain our data. In addition, electron micrographs of real evaporated metallic films indicate that such stepping or terracing is common.

A mathematical model, developed to describe this stepping effect, assumes that the surface is composed of crystallites lying at various slightly skewed angles  $\theta$  to the plane of the mean surface height, as shown in Fig. 16. For mathematical simplicity, it was assumed that the crystallites were square with a characteristic size of  $b \times b$  and that their sides were parallel to crystallite planes. It was also assumed that there were  $b^{-2}$  crystallites per unit surface area and that they were oriented at a randomly varying angle  $\psi$  with respect to the  $\vec{E}$  field of a normally incident light beam. The crystallite size  $b$  was assumed much greater than the characteristic distance  $d$  between steps on the surface. The roughness model, defined in this manner, accounts for the possibility of periodic discontinuities associated with crystallites growing at slightly skewed angles and can be modified easily to describe a surface for which information concerning the mean number of crystal-surface discontinuities is available. If, in fact, it is assumed that an exponential distribution of crystallites over angle  $\theta$  given by  $f(\theta) = (1/\langle \theta \rangle) e^{-\theta/\langle \theta \rangle}$ , then an exact solution for the roughness spectrum of our model surface is obtained as

$$\sigma^2 g(k) = \frac{d_0^2}{\pi k \langle k \rangle} \sum_1^{\infty} \frac{1}{n^3} e^{-k/\langle k \rangle n}, \quad (17)$$

where  $\langle k \rangle = 2\pi \langle \theta \rangle / d_0 \approx 2\pi / \langle d \rangle$  for  $\langle d \rangle \gg d_0$ , and

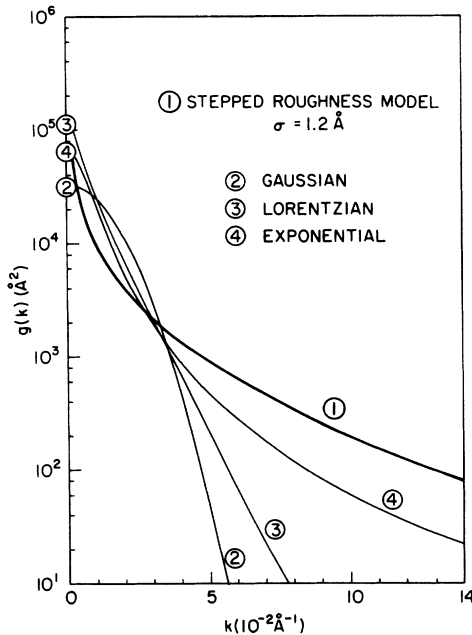


FIG. 17. Stepped-roughness model for Al. The normalized roughness spectrum is plotted for a randomly oriented distribution of crystallites, such as seen in Fig. 16. The crystallites are assumed to have an exponential distribution of distances  $d$  between steps, with a mean stepping distance of  $200 \text{ \AA}$ . The step height is assumed equal to  $4.1 \text{ \AA}$ , the Al lattice constant. Also shown are normalized Gaussian, Lorentzian, and exponential mathematical models for surface-roughness spectra, assuming autocorrelation lengths of  $200 \text{ \AA}$ .

$\langle d \rangle$  is the mean distance between steps. For this model,  $\sigma$  can be shown to equal  $(d_0^2/12)^{1/2} = 1.18 \text{ \AA}$  for Al.

The expression in Eq. (17) is a convergent series in  $n$ , but its value, unfortunately, cannot be expressed as a closed-form function of  $k$ ; however, a reasonably accurate approximation to the above summation can be obtained by assuming

$$\sum_1^{\infty} \frac{1}{n^3} e^{-k/\langle k \rangle n} \approx \int_{1/2}^{\infty} \frac{1}{n^3} e^{-k/\langle k \rangle n} dn. \quad (18)$$

As an approximate expression for the roughness spectrum this integration yields

$$\sigma^2 g(k) = \frac{d_0^2}{\pi} \left[ \frac{\langle k \rangle}{k^3} (1 - e^{-2k/\langle k \rangle}) - \frac{2}{k^2} e^{-2k/\langle k \rangle} \right]. \quad (19)$$

This expression can be integrated over all  $k$  to obtain the rms roughness  $\sigma$ . The value obtained ( $d_0/\pi$ ) is only 1.10 times the correct value for  $\sigma$ , indicating that the approximation to Eq. (17) is fairly accurate.

Figure 17 is a plot of the roughness spectrum  $g(k)$  for a mean stepping distance of  $200 \text{ \AA}$  and  $d_0 = 4.1 \text{ \AA}$ , which is that of Al; also shown are the

Lorentzian, exponential, and Gaussian roughness spectra, assuming autocorrelation lengths of  $200 \text{ \AA}$ . Our stepped roughness model yields the very-high- $k$  spectral components so necessary to explain the experimental data and so lacking in other mathematical roughness models.

(b) *Comparison to residual-roughness photoyield.* The mean stepping distance in Eq. (19) was varied so that calculations of photoyield from the stepped roughness model, assuming the surface-effect photoemission strength shown in Fig. 13, would yield theoretical values in agreement with the experimental values in Fig. 15. Plasmon broadening in the Elson-Ritchie theory was compared to a greater plasmon broadening, and a best fit was obtained by using plasmon broadening 2.5 times that predicted by Elson and Ritchie and a mean stepping distance of  $200 \text{ \AA}$ . A comparison of this optimal theoretical curve to experiment is shown in Fig. 18; also shown is the theoretical curve that assumes the same stepping distance and the normal Elson-Ritchie plasmon broadening. Significantly, the optimal match to experiment had an associated theoretical reflectance drop of  $\sim 0.7\%$  at the surface-plasma frequency. Our theoretical model, therefore, not only is in good agreement with our photoyield measurement, but is also consistent with smooth surface reflectance measurements that indicate residual-roughness reflectance drops of less than  $1\%$ .

The inability of the normal plasmon broadening in the Elson-Ritchie theory to agree with experiment is significant. It has been noted that their plasmon-broadening effects are not strong enough to explain experimentally observed broadening. Nowhere is this more apparent than in the broadening observed in residual-roughness photoyield. Ritchie has suggested<sup>29</sup> that roughness-induced elastic scattering of the high- $k$  plasmons might cause the additional lifetime broadening of plasmons, but one would expect such effects to be insignificant in our smoothest films. Two alternative explanations exist. The first is that the reflectance drops and photoyield increases extending above the surface-plasma frequency may be caused by hydrodynamic dispersion effects so important for very-high- $k$  plasmons.<sup>30</sup> A quantitative evaluation of this effect is obscured by theoretical uncertainty as to the precise effect of hydrodynamic dispersion on the plasmon-dispersion curve.<sup>29</sup>

A second explanation is that a dominant broadening mechanism in these high- $k$  plasmons is the surface-photoemission decay process, which was prominent in our photoyield results. The Elson-Ritchie plasmon-broadening mechanism is a volume-decay process and ignores the plasmon excitation of electrons at the surface. The extremely high photoyield per decaying plasmon ( $0.3 \text{ elec}$ -

trons) derived from the yield and reflectance measurements on our smoothest film strongly imply that surface photoexcitation, known to dominate the observed photoemission from this film, must actually be significant in the plasmon decay as well. With this strong additional loss mechanism, the lifetime broadening of the high- $k$  plasmons, of necessity, must be much greater than in the simple volume-decay theory.

One of the most interesting aspects of the success of our stepped roughness model in explaining "smooth" surface photoyield is the implication that the discrete stepping of the surface introduces relatively strong high- $k$  spectral components in even very smooth films. The relative importance of these high- $k$  components should increase as one goes to smoother films and, as a result, plots of the *normalized* roughness spectra  $g(k)$  should reveal absolute increases in their high- $k$  spectra. This interpretation is consistent with the experimental observations of derived  $g(k)$  vs film roughness discussed in Paper I. In fact, the normalized derived roughness spectra have been replotted in Fig. 19 for the  $\sigma = 12, 18,$  and  $22 \text{ \AA}$  films discussed in Paper I; the normalized stepped roughness spectrum is also shown for a mean stepping distance of  $200 \text{ \AA}$ . These plots indicate the systematic increase in the high- $k$  spectral components of the normalized spectra as one goes from the  $22\text{-\AA}$  roughness to a physical model of our smoothest films.

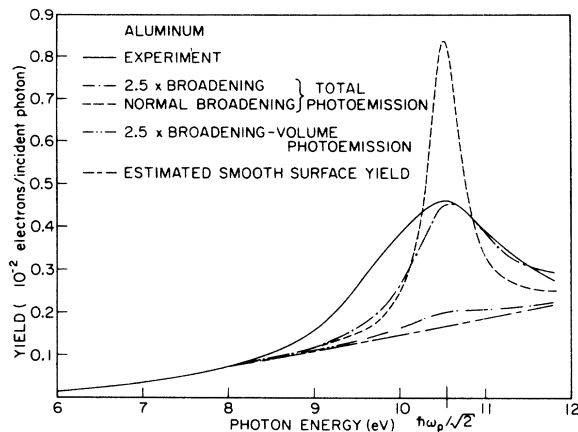


FIG. 18. Match of the stepped-roughness model to minimum observed Al photoyield. The roughness spectrum in Fig. 17 gave the match to experiment. The calculation utilized the surface- plus volume-effect photoemission expression of Eq. 13, assuming 2.5 times normal plasmon broadening and the characteristic surface-effect strength  $Y_c$  (fitted). Also shown is the photoyield calculated from this roughness model, assuming normal plasmon broadening, and assuming that only the volume photoeffect is involved.

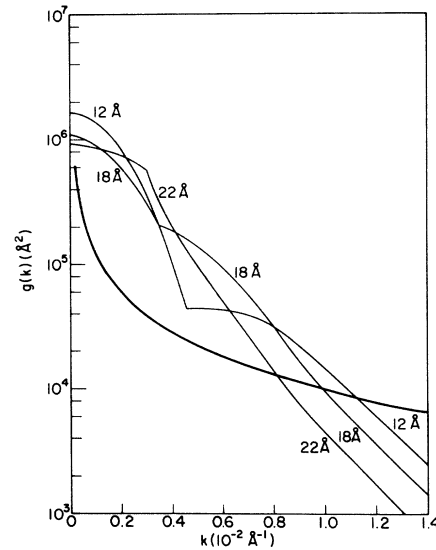


FIG. 19. Comparison of the normalized stepped-roughness model spectrum of Fig. 17 to normalized roughness spectra derived from experiment for three films described in Paper I. The comparison indicates that the discrete stepping of the surface associated with a finite lattice constant tends to introduce high- $k$  spectral components that become more important in the smoother films.

### 3. Annealing Effects

One significant result of our roughness-dependent photoyield studies was the observation of a strong time dependence in the photoyield from our slightly roughened films. This observation served to further confirm the high sensitivity of photoyield to surface roughness and also served to suggest a very effective new tool for the study of surface atomic mobility. The most reasonable explanation of this observation is that we see a decrease in roughness-aided optical coupling to surface plasmons, which is associated with the room-temperature annealing of Al surfaces. This is supported by Feuerbacher's observation<sup>21</sup> of from 1 to 3% increases in Al reflectance values near 10 eV during the first 15 min following evaporation.

Figure 20 is an example of this effect, in which photoyield vs time is plotted for an Al film irradiated with a 10.2-eV light. The strong suggestion of room-temperature annealing effects immediately following film evaporation prompted higher-temperature annealing at 10 and 24 h after film preparation. The film was evaporated at  $55 \text{ \AA}/\text{sec}$  onto a bowl-feed polished-quartz substrate. Evaporation pressure was  $7\text{--}8 \times 10^{-9}$  Torr, and measurements were taken at  $1\text{--}2 \times 10^{-11}$  Torr. The drop in yield immediately following evaporation is qualitatively consistent with the reflectance observations

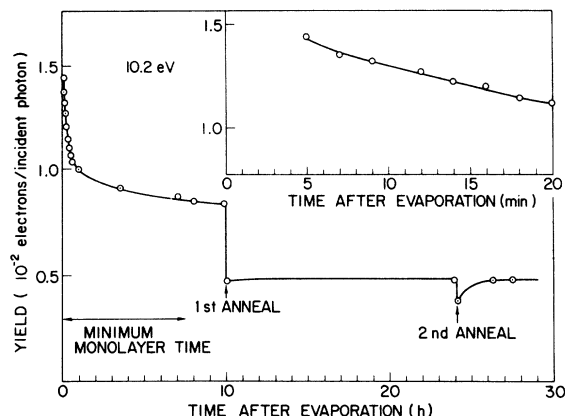


FIG. 20. Al photoyield at 10.2 eV as a function of time and annealing procedures. Minimum monolayer time was calculated for a  $2 \times 10^{-11}$ -Torr base pressure, assuming the base-pressure gas constituents given in Ref. 19.

of Feuerbacher.

The first anneal was carried out by heating the quartz substrate and substrate holder until the holder temperature rose to 100 °C; this temperature was maintained for approximately 10 min. Temperature of the film could not be monitored; however, we believe that it may have risen to 200–400 °C. During this 10-min anneal, the pressure reached a maximum of  $3 \times 10^{-10}$  Torr.

The striking drop in photoyield associated with this first anneal and the lack of any variation during the following 12 h are consistent with our belief that the photoyield changes are strongly related to changes in surface roughness.

It can be assumed that there is some configuration of Al atoms on the surface that yields a lowest energy for the Al film. This configuration could be based on the underlying Al crystallite growth patterns and would not be a surface that minimizes roughness. The preferred state, however, might very well be considerably smoother than the originally deposited film. In such circumstances, the surface roughness would be expected to decrease slowly following evaporation and to decrease abruptly on annealing.

A second anneal was carried out approximately 14 h following the first. The length and temperature were the same as in the first anneal, but the pressure during heating reached only  $8 \times 10^{-11}$  Torr. Again, the abrupt drop in yield followed by a slow return to the preanneal values are strongly suggestive of our proposed model. If a minimum energy surface was achieved during the first anneal which was not, in fact, a minimum-roughness surface, further annealing might lower the roughness, but the roughness and thus the photoyield would be expected to return slowly to their values before the second anneal. The importance of roughness

changes can be further verified by studying the spectral variations in the Al-film photoyield during the aging and annealing processes described by Fig. 20; such yield spectra are shown in Fig. 21. It should be noted that the lowest photoyield spectrum (obtained immediately following the second film anneal) is the “minimum” experimental photoyield shown in Fig. 15 and used to estimate our smooth surface Al yield.

One important question is whether the photoyield decreases are associated with surface contamination with time or surface contamination with annealing. Kinetic theory predicts that significant surface contamination is simply not possible at our operation pressures (minimum calculated monolayer time shown in Fig. 20 assumes a unit-sticking coefficient). Even if surface contamination is possible, however, it has been shown<sup>31</sup> that such contamination tends to increase rather than decrease the photoyield of Al. Despite these arguments, the known strong sensitivity of photoyield to surface contamination should motivate a closer examination of these possible effects which probably are seen most easily in the electron distribution curves (EDC's) of the photoyield. Even surface contamination of less than a monolayer has been known to distort substantially the EDC's of certain materials.<sup>32</sup> Generally, contamination effects manifest themselves as large low-energy peaks in the EDC's, associated with the scattering of photoexcited electrons as they escape through the contaminated surface.

In Fig. 22, the EDC's are seen at several excitation energies of an Al film just prior to and immediately following anneal. It can be noted from

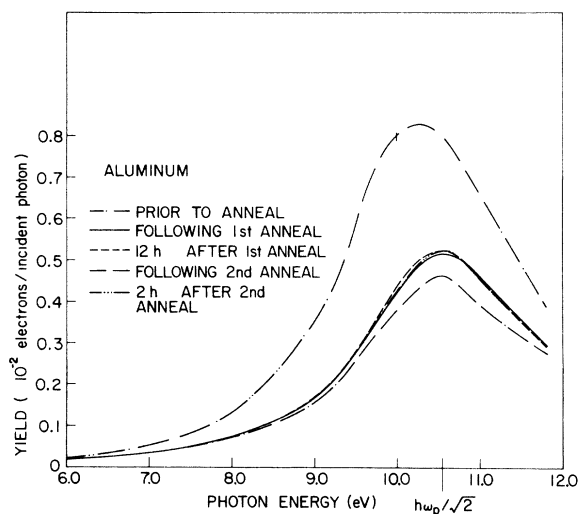


FIG. 21. Al photoyield vs photon energy, time, and annealing procedures. The sample studied is described in Fig. 20.

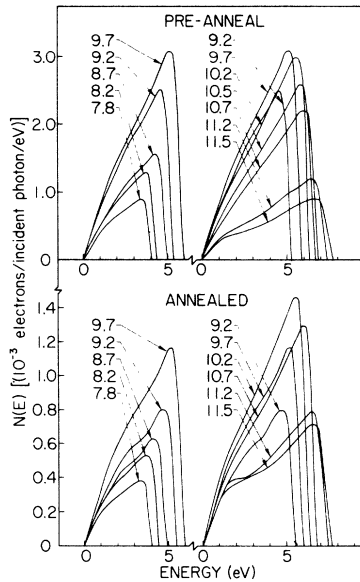


FIG. 22. Photoemission electron-distribution curves for an Al sample prior to and following annealing of the Al film. EDC's are plotted for several photon-excitation energies, and two vertical scales are used for the two sets of data.

the change in the vertical photoyield scale that a substantial drop occurs in the magnitude of the yield during the annealing process; nevertheless, there is very little indication of an increase in the number of low-energy scattered electrons in the annealed film and, as a result, no strong indication that surface contamination occurs during annealing.

It is interesting to note that the only real indication of low-energy scattered electrons in any of the EDC's occurs at excitation frequencies above the surface-plasma frequency and appears slightly stronger in the annealed film. The EDC's at excitation frequencies of 11.2 and 11.5 eV are replotted (Fig. 23) and compared to the 10.2-eV EDC; the curves are of arbitrary magnitude for easy comparison. The appearance of scattered electrons at excitation  $h\nu$  above  $\hbar\omega_p/\sqrt{2}$  is consistent with our interpretation of the plasmon-decay process as predominantly a surface-photoemission effect. In the surface theory, electrons are excited at the surface and immediately escape; they cannot create a secondary or scattered electron prior to being emitted. Only in the volume-photoemission theory can electrons create secondary or scattered electrons during transit toward the surface, and only at frequencies removed from  $\hbar\omega_p/\sqrt{2}$  can the volume-photoemission effect begin to dominate the photoemission process.

Although the appearance of scattered electrons in the EDC's above  $\hbar\omega_p/\sqrt{2}$  can be attributed to mech-

anisms other than the one proposed and thus should not be extended too far, a similar emergence of scattered electrons in EDC's just above the surface-plasma frequency has been observed by Gesell and Arakawa<sup>33</sup> in photoemission experiments on Mg.

## V. CONCLUSIONS

Photoyield measurements on Al films of varying measured roughness indicate very strong peaks in photoyield per incident photon at energies approaching the surface-plasma frequency  $\hbar\omega_{sp} = 10.55$  eV. The magnitudes of these peaks are strongly correlated to surface roughness.

Attempts have been made to explain this photoyield effect in terms of a two-step process. In the first step, surface roughness allows optical excitation of surface plasmons in accordance with the surface-plasmon excitation theories described in Paper I.<sup>1</sup> In the second step, the surface plasmon is assumed to decay primarily through one-electron excitations, and these excitations, directly analogous to photoexcitations, result in increases in photoyield.

Two mechanisms were proposed to explain this surface-plasmon one-electron decay. It was assumed first that the observed plasmon-induced photoemission of electrons was caused primarily by the excitation of electrons associated with the penetration of plasmon fields within the volume of the metal. This is analogous to the "volume" theory of photoexcitation which assumes electronic momen-

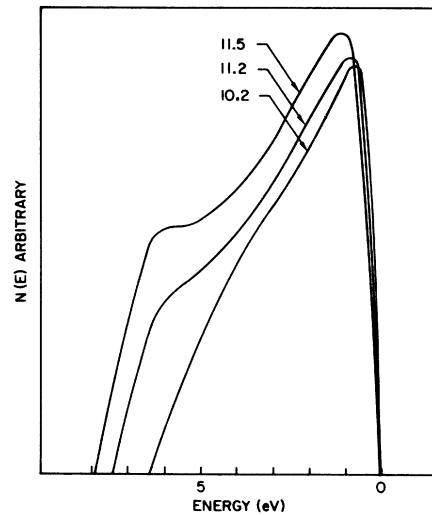


FIG. 23. Plots of three EDC's for the annealed film of Fig. 22. Note the appearance of what are probably low-energy secondary (scattered) electrons for the 11.2 and 11.5 eV excitation energies that lie above the surface-plasma frequency. Curves are arbitrarily normalized for ease of comparison.

tum conservation within the volume of the metal; however, it was found that the experimentally observed photoyield per excited surface plasmon was far too great to be explained by this commonly accepted theory.

The failure of the volume theory and some very unique aspects of the associated surface-plasmon fields strongly suggested that a process directly analogous to the historically significant surface-effect photoemission dominated the observed plasmon-decay process. Surface-effect photoemission assumes that momentum conservation in an electronic excitation can occur only at the surface and in a direction normal to the surface. This implies that surface-effect photoexcitation can occur only if there are strong components of the excitation field lying normal to the surface, a criterion not easily met in the type of near-normal-light-incidence photoemission experiments carried out in recent years. This surface effect can result, however, from any process having associated excitation field components normal to the surface; it can result from an optical excitation incident at an oblique angle on a smooth surface, or it can arise from excitation by surface-plasmon fields which have extremely strong components normal to the surface. In a sense, *plasmon-induced surface-effect photoemission can be thought to stem from the roughness-aided conversion of a normally incident photon having no field components normal to the surface to a surface-plasmon having strong field components normal to the surface.* This surface photoemission effect can be enhanced appreciably by strong concentration of energy near the surface, which occurs when high- $k$  surface plasmons are excited.

Because the surface photoeffect can result from any mechanism that presents strong excitation fields normal to the surface, the surface-effect strength can be defined uniquely in terms of a characteristic photoyield per unit normal field strength. The actual photoyield, therefore, can be expressed in terms of this characteristic surface-effect photoyield  $Y_c(\hbar\omega)$  and the field strength of the excitation mechanism (either a decaying surface plasmon or an obliquely incident optical field). As a result, although the photoyield per decaying surface plasmon in the volume theory could be uniquely calculated, the photoyield in our surface-effect theory remains in terms of the characteristic surface-effect strength  $Y_c(\hbar\omega)$ . Attempts have been made to determine theoretically the spectral dependence of  $Y_c(\hbar\omega)$  for free-electron metals (notably the work of Mitchell<sup>4,11</sup>), but these attempts have relied critically on the details of potential discontinuity at the surface and have ignored the interference effects between volume and surface photoexcitations suggested by Schaich and Ash-

croft.<sup>13</sup> Theoretical calculations have made use of several questionable assumptions concerning variations in excitation fields near the surface.

In our investigation, we *chose* a characteristic surface-effect strength  $Y_c(\hbar\omega)$  which was in good agreement with experimentally observed photoyield per decaying plasmon; that is, our surface-photoeffect plasmon-decay theory was used to explain the experimental results by fitting the unknown parameter  $Y_c(\hbar\omega)$  to them. This fit obtained a characteristic surface strength comparable at lower energies ( $\approx 6$  eV) to the values determined by Mitchell but noticeably greater at higher energies. Calculations on various refinements of the Mitchell theory<sup>4,11,12,34</sup> are under way in the hopes of obtaining better agreement with the experimentally determined surface-effect strength.

The acceptability of our interpretation of the plasmon-decay process as a surface-photoexcitation process is strengthened by two additional observations. First, it was noted that a single derived spectral dependence for  $Y_c(\hbar\omega)$  could obtain agreement with experiment for several different film roughnesses; second, an independent type of measurement of  $Y_c(\hbar\omega)$  for  $\hbar\omega = 7.8$  eV yielded a value for  $Y_c$  that was within 20% of the value determined from our plasmon-decay measurements at this energy. In this independent determination of  $Y_c(\hbar\omega)$ , photoyield was measured as a function of angle-of-light incidence for  $p$ -polarized light incident on one of the smoothest Al surfaces that we were able to prepare. Experimental constraints restricted this determination to the single energy of 7.8 eV;  $Y_c(\hbar\omega)$  is characteristic of the surface strength and independent of excitation process so that  $Y_c(7.8$  eV) could be fitted to experimentally observed photoyield vs angle-of-light incidence just as it could be fitted to the plasmon-decay data. Contributions from the volume-photoemission effect and optical-constant effects were included in the calculations.

Our observations and interpretations serve to provide what is believed to be the first strong evidence for the existence of the historically significant surface-effect photoemission. Our measurements permitted the first experimental estimate of the relative strength of the surface- and volume-photoemission effects. The derived values for the relative strengths of these two photoexcitation processes in Al indicate that the volume-photoeffect process would dominate the photoemission measurements over the spectral range if it was not for the intermediate roughness-aided excitation of surface plasmons. Specifically, using these effects, and ignoring plasmon excitation, we calculated that light in a cone of half-angle  $10^\circ$  at near-normal incidence on a very smooth Al film would excite surface- and volume-effect photoemission in a ratio

of less than 1 : 30. It was argued that the relative strength of the surface effect should be even weaker for near-normal-incident light on the very smooth surfaces of other metals.

It should be emphasized that all of the discussions in this paper are based on the assumption of a specular process in which the momentum of the electron or the field distribution of the incident electromagnetic radiation is not randomized because of the influence of the surface. The results of the off-normal polarized-light experiment would tend to verify this assumption for Al; however, Sutton<sup>35</sup> has shown that, if the specular condition is relaxed, many of the arguments in this paper break down.

Among the most interesting and practical effects associated with this highly sensitive roughness-induced photoyield increase are what we have called annealing and residual-roughness effects. Photoyield near the surface-plasma energy was so sensitive to surface roughness that film smoothing associated with room-temperature annealing of the Al was sufficient to cause a marked decrease in photoyield with time; this decrease could be accelerated by heating the films. Conclusive evidence was presented to indicate that the photoyield drop could not be associated with surface contamination of the film with time or with heating. This evidence included the measurement of the associated photoyield EDC's for the Al films just prior to and just after heating the film.

The residual-roughness effect manifested itself as a significant increase in photoyield at the exact surface-plasma frequency in even our smoothest Al films, but such a strong effect was not noted in the reflectance. This evidence suggests a significant enhancement in photoyield per decaying surface plasmon for these smooth surfaces, an effect that might be explained in terms of a preferential

excitation of high- $k$  plasmons in the smoother films. It became apparent from our theory of plasmon-induced photoyield increases that these high- $k$  plasmons show the greatest photoyield per decaying plasmon.

A mathematical model was proposed to describe roughness spectra of relatively smooth surfaces, based on the discrete stepping of the surface associated with the finite lattice constant of real metals. The spectrum of this stepped-roughness model was uniquely specified by a mean distance between surface-height steps, with each step equal to the metallic lattice constant (4.1 Å for Al). The sharp variations in surface height obtained the type of high spatial frequency-height variations so necessary in allowing optical coupling to high- $k$  plasmons. Our model was fitted to our residual-roughness photoyield measurements and gave excellent agreement with measurement for the realistic mean stepping distances of  $\approx 200$  Å.

Our success of interpreting the observed optical measurements reported in Paper I and the success of our surface-plasmon-surface-photo-effect theory in interpreting observed photoyield measurements may prove extremely useful in future attempts at surface-roughness characterization such as the annealing and residual-roughness effects described. It also indicates that explanations of photoemission from Al, In, and the alkali metals that neglect the surface-plasmon-surface-photo-emission mechanism should be reexamined.

#### ACKNOWLEDGMENTS

The authors wish to acknowledge the valuable assistance of Dr. H. E. Bennett, Dr. J. L. Stanford, and Dr. R. H. Ritchie in the measurements and interpretation of the optical properties of rough metallic surfaces. We are grateful also to Dr. Leon Sutton for his valuable discussions.

\*Work supported by the Advanced Research Project Agency through the Center for Materials Research, Joint Services Electronics Program, National Science Foundation at Stanford University, Stanford, Calif. 94305.

<sup>1</sup>J. Endriz and W. E. Spicer, preceding paper, *Phys. Rev.* **4**, xxx (1971).

<sup>2</sup>J. Endriz and W. E. Spicer, *Phys. Rev. Letters* **24**, 64 (1970).

<sup>3</sup>I. Tamm and S. Schubin, *Z. Physik* **68**, 97 (1931).

<sup>4</sup>K. Mitchell, *Proc. Roy. Soc. (London)* **146A**, 442 (1934).

<sup>5</sup>J. M. Elson and R. H. Ritchie, *Phys. Letters* **33A**, 255 (1970).

<sup>6</sup>J. Crowell and R. H. Ritchie, *J. Opt. Soc. Am.* **60**, 794 (1970).

<sup>7</sup>Fröhlich, *Ann. Physik* **7**, 103 (1930).

<sup>8</sup>H. Y. Fan, *Phys. Rev.* **68**, 43 (1945).

<sup>9</sup>W. E. Spicer, *Phys. Rev.* **112**, 114 (1958).

<sup>10</sup>This is an approximate expression where it is assumed

that (i) the electron-electron scattering process dominates all other scattering processes and (ii) the scattered electrons do not have sufficient energy to escape.

<sup>11</sup>K. Mitchell, *Proc. Roy. Soc. (London)* **153**, 513 (1935).

<sup>12</sup>L. I. Schiff and L. H. Thomas, *Phys. Rev.* **47**, 860 (1935).

<sup>13</sup>W. L. Schaich and N. W. Ashcroft, *Phys. Rev. B* **3**, 2452 (1971).

<sup>14</sup>For example, Eq. (1) shows that the change in the normal component of the plasmon fields in going from the vacuum to the metal occurs over a distance  $\Gamma^{-1}$  from the surface. This distance is found to be on the order of 1 Å for surface plasmons of interest, a distance comparable to the excitation region of the surface effect.

<sup>15</sup>W. F. Krolikowski, Ph.D. thesis (Stanford University, 1967) (unpublished).

<sup>16</sup>R. Koyama, Ph.D. thesis (Stanford University, 1969), Appendix A 3 (unpublished).

<sup>17</sup>J. L. Stanford, H. E. Bennett, J. M. Bennett, E. J. Ashley, and E. T. Arakawa, *Bull. Am. Phys. Soc.* **13**, 989 (1968).

<sup>18</sup>Modified form of the results of Ref. 17, and obtained from J. L. Stanford (private communication).

<sup>19</sup>J. Endriz, Ph.D. thesis (Stanford University, 1970) (unpublished).

<sup>20</sup>See the discussion of the uv light polarizer in G. Derbenwick, Ph.D. thesis (Stanford University, 1970) (unpublished).

<sup>21</sup>B. P. Feuerbacher and W. Steinman, *Opt. Commun.* **1**, 81 (1969).

<sup>22</sup>H. E. Bennett and J. C. Porteus, *J. Opt. Soc. Am.* **51**, 123 (1961).

<sup>23</sup>Reference 16, Chap. 3.

<sup>24</sup>F. Wooten, T. Huen, and R. N. Stuart, in *Optical Properties and Electronic Structure of Metals and Alloys*, edited by F. Abeles (North-Holland, Amsterdam, 1966), p. 332.

<sup>25</sup>W. E. Spicer and W. F. Krolikowski, *Phys. Rev.* **185**, 882 (1969).

<sup>26</sup>W. E. Spicer and W. F. Krolikowski, *Phys. Rev. B* **1**, 478 (1970).

<sup>27</sup>F. Wooten (private communication).

<sup>28</sup>The very high photoyield of  $\sim 0.3$  electrons/(decaying plasmon) in this surface-effect process obviously negates our assumption that volume-effect photoexcitation dominates the plasmon energy-loss process. For the high- $k$  plasmons of these smooth films, the surface photoexcitation must be a dominant energy-loss mechanism. The implications of this breakdown in the assumptions leading to Eq. (13) are not pursued.

<sup>29</sup>R. H. Ritchie (private communication).

<sup>30</sup>R. H. Ritchie and R. E. Wilems, *Phys. Rev.* **178**, 372 (1969).

<sup>31</sup>B. Feuerbacher, M. Skibowski, and W. Steinman, *J. Opt. Soc. Am.* **58**, 137 (1968).

<sup>32</sup>W. E. Spicer, in *Optical Properties of Solids*, edited by F. Abeles (North-Holland, Amsterdam, to be published).

<sup>33</sup>T. F. Gesell and E. T. Arakawa (private communication).

<sup>34</sup>K. Mitchell, *Proc. Cambridge Phil. Soc.* **31**, 416 (1935).

<sup>35</sup>L. Sutton, *Phys. Rev. Letters* **24**, 8 (1970); **24**, 386 (1970).

## The de Haas-van Alphen Effect in Lutetium<sup>†</sup>

J. A. Hoekstra and R. A. Phillips\*

*Institute for Atomic Research and Department of Physics, Iowa State University, Ames, Iowa 50010*

(Received 22 July 1971)

de Haas-van Alphen oscillations have been observed in lutetium single crystals using high impulsive magnetic fields. A single-frequency branch is reported which has a minimum value of 3.75 MG along the  $c$  axis and extends  $\sim 22^\circ$  in both the  $(1\bar{2}10)$  and  $(\bar{1}100)$  planes. Comparison of the experimental results with the relativistic-augmented-plane-wave Fermi surface of Loucks suggests that the electron columns are pinched off at the symmetry point  $H$ .

The de Haas-van Alphen (dHvA) effect in Lu single crystals has been studied in pulsed fields up to 200 kG. It is believed that the data presented here are the first direct experimental information related to the Fermi surface (FS) of any trivalent heavy-rare-earth metal.<sup>1</sup> The experimental procedure and data-reduction techniques used in the present investigation are essentially the same as those reported by Girvan *et al.*<sup>2</sup> and will not be discussed here.

The crystal structure of Lu is hexagonal close packed (hcp) and single crystals were prepared by the electrotransport technique.<sup>3</sup> The starting material had a resistivity ratio ( $\rho_{300}/\rho_{4.2K}$ ) of  $\sim 21$  and consisted of a  $\frac{1}{8}$ -in. rectangular rod 4 in. long. This rod had been spark cut from a single-crystal slab of Lu prepared by the arc-zone-melting technique<sup>4</sup> and annealed in a high vacuum for several hours. During the transport process the Lu bar was held at a temperature of 1120°C in a vacuum

of  $10^{-10}$  Torr for 166 h. Two rectangular samples  $\frac{1}{2}$  mm on a side and 4 mm long were cut from the transported rod, which had a resistivity ratio of  $\sim 60$ .

Figure 1 shows the angular dependence of the observed dHvA frequency branch, which has a minimum value of  $F = 3.75$  MG and an effective mass of  $0.38 \pm 0.05$  (in units of the free-electron mass) when the field is along [0001]. The oscillations are only observed for field directions within  $22^\circ$  of [0001] and disappear abruptly at this angle. Such behavior indicates that, due to the geometrical features of the FS, the orbit exists only within  $22^\circ$  of [0001]. The solid curves in Fig. 1 are a calculated fit to the data using the equation

$$F = F_0 / (1 - D \tan^2 \theta)^{1/2}, \quad (1)$$

where  $F_0 = 3.75$  MG and  $D = 1.83$  for the  $(\bar{1}100)$  plane and 2.12 for the  $(1\bar{2}10)$  plane. This equation expresses the angular dependence of a dHvA frequency